SPIN EFFECTS IN HADRONIC COLLISIONS AT LARGE MOMENTUM TRANSFERS*

By J. Szwed

Institute of Computer Science, Jagellonian University, Cracow**

(Received June 16, 1982)

The role of spin in hadron-hadron collisions at large $p_\perp$ is investigated. The short distance diagrams and the end-point ($x \to 1$) contribution give phenomenologically similar results for the elastic nucleon-nucleon differential cross-section but differ significantly when looking at the spin-spin asymmetries. The spin analysis suggests the dominance of the end--point diagrams at large angles and present energies. The limits on the nucleon wave function are obtained from the comparison of spin effects in exclusive and inclusive reactions. Higher order results in exclusive channels are reviewed. In the inclusive production we propose a simple model of baryon polarization at large transverse momentum which accounts qualitatively for all experimental data in these processes. Other models are also reviewed. The whole investigation suggests that the spin effects are a relatively clear probe of the complicated hadron dynamics.

PACS numbers: 13.85.-t

1. Introduction

When looking at the complicated structure of hadron-hadron scattering it is important to investigate all possible observables which characterize these processes. It may turn then out that some quantities define uniquely the underlying dynamics whereas the others come out similar in various calculation techniques. The following paper is devoted to the investigation of the role of spin observables in hadronic collisions. Most of the work concerns exclusive processes and in particular elastic scattering. In these channels it is believed that we are able to separate the hard part of the process at large momentum transfer t, in analogy to deep inelastic scattering. We present three, potentially important contributions to elastic scattering. They differ by the way the soft and hard parts are separated. In the first one [1] the hard process contains in the lowest order all valence quarks which exchange far off-shell gluons. The second contribution [2] — a special configuration of the first one — occurs when all interacting constituents scatter with the exchange of equal momentum transfers (pinch contribution). These diagrams are absent in the formfactor

* This paper is presented as the qualifying thesis for habilitation in Jagellonian University.

** Address: Instytut Informatyki UJ, Reymonta 4, 30-059 Kraków, Poland.

calculation. The third one comes from the configuration when one of the constituents in the hadron carries almost all its momentum ($x \to 1$), the hard part contains in this case only the fast constituents (end-point contribution [3]). The extension [4] of Drell-Yan-West relations to elastic scattering follows from the last contribution. In the situation when the relative normalization of the mentioned terms is not fixed — it is given by the unknown, soft part of the process — the importance of each term is determined phenomenologically. It turns out that the calculated spin-spin asymmetries form a clear-cut test of the underlying dynamics.

Another process investigated in detail is the large $p_\perp$ baryon production. Here again the spin quantities turn out to show up interesting effects, in particular the hyperon polarization which increases with the transverse momentum.

Both the spin-spin asymmetries in elastic scattering and the hyperon polarization were a challange to the theorists [5], after their measurements were first published [6, 7]. As a matter of fact their unexpected behaviour caused the author to get interested in the spin effects of hadron physics.

The paper is organized as follows. In Section 2 we review the short distance expansion applied to the exclusive processes starting with the electromagnetic formfactor of the meson where the situation is best known. We also discuss the elastic scattering concentrating on the spin-spin asymmetries. Section 3 is devoted to the pinch singularity diagrams of elastic scattering and its role at large t. The Drell-Yan-West relations following from the end-point region are recalled in Section 4. They are also extended there to the elastic scattering. In the last case one is also able to calculate the explicit form of the amplitude in the leading order, so we compare it with all elastic NN, $\overline{\text{NN}}$ and π N data obtaining very good agreement. The crucial step is the evaluation of the spin-spin asymmetries which suggest, when compared with the data on A_{nn} [6], that the end-point contribution dominates the large c.m. angle region at present energies. As we already mentioned the results in elastic scattering depend partly on the soft wave function. We test this dependence in the last part of Section 4 by comparing the information coming from deep inelastic and elastic scattering. A definite pattern of SU(6) symmetry breaking in the nucleon wave function emerges.

Higher order corrections are briefly reviewed in Section 5. They are fully under control in the pion formfactor but some conjectures are also made for the elastic amplitude. One of the theoretical diseases, which makes our phenomenological analysis legitimate, is the lack of information on the scale in these processes, in particular on the one governing the Sudakov effects.

In Section 6 we skip to another type of hadronic processes where the spin effects show up in a nontrivial way. We propose a phenomenological simple mechanism of baryon polarization at large $p_\perp$ based on multiple quark scattering which accounts qualitatively for all existing data and present its predictions. Other existing models are also reviewed.

Summary and conclusions follow in Section 7. We stress there once more the role of spin in large momentum transfer collisions. Its effect is very pronounced in the hard part of scattering and survives in a comparatively clean way the convolution with the soft part.

2. *Short-distance amplitudes in exclusive processes*

Recently it has been shown [8] that some exclusive processes can be analyzed in perturbative QCD. This means that one is able to factorize the large scale (Q^2) dependence from the soft momentum scale (p^2) in the corresponding amplitude $\mathscr{T}(Q^2, p^2)$:

$$\mathscr{T}(Q^2, p^2) = \frac{1}{Q^N}\left[T(Q^2/\mu^2, \alpha_s(\mu^2)) \otimes f(\mu^2, p^2) + R(Q^2, p^2)\right],$$

where N is the dimension of $\mathscr{T}$, R is power-suppressed with respect to the convolution $T \otimes f$ and μ is the boundary between large and small momenta. Full control over the perturbation expansion means that the renormalization group equation is valid for the coefficient function (hard part of the process). Up to now the latter step was proven [8] only in the case of meson formfactors. In other processes, like the baryon formfactors or fixed angle elastic scattering higher order corrections, essentially Sudakov effects (discussed in Section 5), can spoil the validity of the leading order results.

A. Formfactors

The pion formfactor to leading order in m_q^2/Q^2 (m_q is the quark mass) and all orders in $\alpha_s(Q^2/\Lambda^2)$ takes the form [8] (see Fig. 1a)

$$F(Q^2) = \int [dx]\,[dy]\,\Phi^+(x, \tilde{Q}_x) T_H(x, y, Q) \Phi(y, \tilde{Q}_y) \tag{2.1}$$

with

$$\tilde{Q}_x = Q \cdot \min(x_i)$$

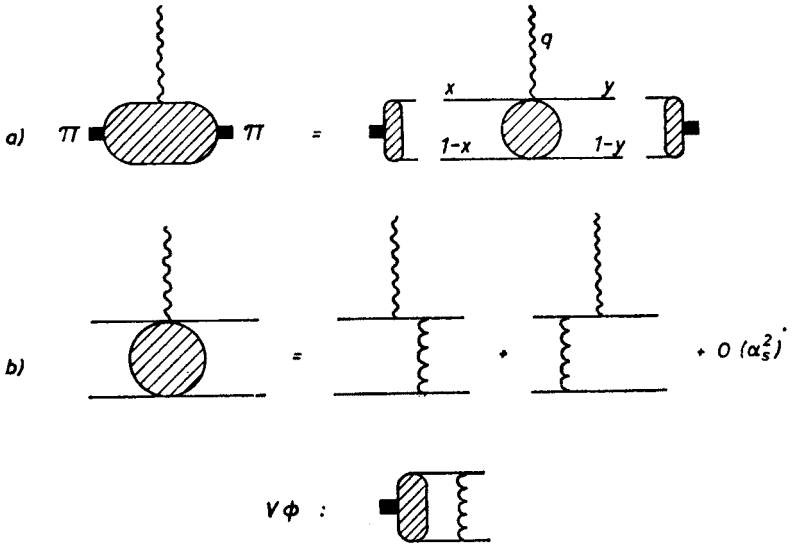

Fig. 1a) The meson formfactor; b) the kernel V of Eq. (2.3) in lowest order

and

$$[dx] = \delta(1-\sum_{i=1}^{2} x_i)\prod_{i=1}^{2} dx_i.$$

T_H is the hard scattering amplitude for the process $\gamma^*q\bar{q} \to q\bar{q}$. It can be expanded in powers of α_s with the leading term being

$$T_H = 16\pi C_F \frac{\alpha_s(Q^2)}{Q^2}\left[\frac{e_1}{x_2 y_2} + \frac{e_2}{x_1 y_1}\right][1+O(\alpha_s)] \tag{2.2}$$

where e_i is the charge of the i-th quark.

The distribution amplitude

$$\Phi(x, \tilde{Q}_x) = 16\pi^2 \prod_{i=1}^{2} \frac{1}{\sqrt{d_i(Q^2)}} \int_0^{\tilde{Q}^2} \prod_{i=1}^{2} \frac{d^2k_{\perp i}}{16\pi^3}\, \delta\left(\sum_{i=1}^{2} k_{\perp i}\right) \Psi(k_{\perp i}, x_i)$$

obeys "the evolution equation" analogous to the Altarelli-Parisi equation [9] for the structure function

$$\frac{\partial}{\partial \log Q^2}\Phi(x, Q) = \frac{\alpha_s(Q^2)}{4\pi}\int [dy] V(x, y)\Phi(y, Q). \tag{2.3}$$

The kernel V stands in the leading order for the one gluon exchange between the $q\bar{q}$ pair (see Fig. 1b). Substituting Eq. (2.2) and the solution of Eq. (2.3) into Eq. (2.1) one obtains the leading order in α_s and m_q/Q^2 expression for the pion formfactor which asymptotically, as $Q^2 \to \infty$, reads [10]

$$F(Q^2) = 16\pi f_\pi^2 \frac{\alpha_s(Q^2)}{Q^2}. \tag{2.4}$$

The normalization is known in Eq. (2.4) because the unknown matrix element $\langle 0|J^\mu|\pi\rangle$ has been expressed by the π weak decay constant f_π.

Analogical result was obtained [11] in leading order for the baryon magnetic formfactor. At asymptotic Q^2

$$G_M(Q^2) \underset{Q^2\to\infty}{\sim} \left[\frac{\alpha_s(Q^2)}{Q^2}\right]^2 \left(\ln\frac{Q^2}{\Lambda^2}\right)^{-4(33-2n_f)/9} \tag{2.5}$$

where n_f is the number of flavours.

At finite Q^2 more terms contribute to (2.5) and the precise shape depends on the distribution amplitude $\Phi(x, Q_0)$ at some Q_0. For example [11], with $\Phi(x, 2\,\mathrm{GeV}^2) \sim \delta(x_1 - 1/3)\cdot\delta(x_2 - 1/3)$ the resulting curves for various choices of Λ_{QCD} are shown in Fig. 2 together with the data [12]. One sees that the corrections to the old dimensional counting rules [13] are not seen, which means that only very small Λ_{QCD} is acceptable.

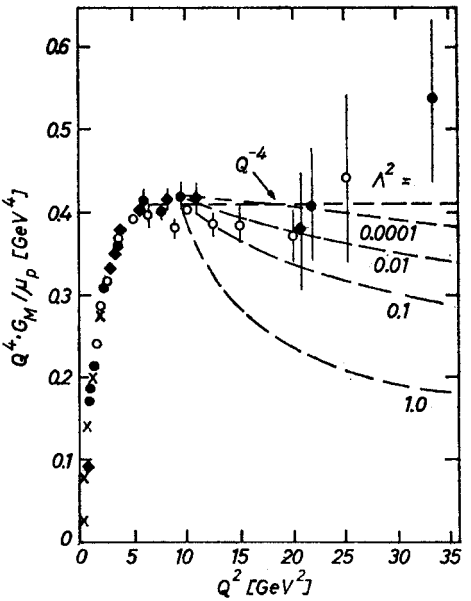

Fig. 2. The magnetic formfactor G_M [12] together with the predictions of Ref. [11]

Another lesson from Fig. 2 is that one does not expect the formfactor to be well described with hard scattering techniques for $Q^2 < 5$ GeV^2 — this value of the momentum transfer seems to be a borderline between soft and hard scattering.

The spin structure of the formfactors is very simplified in the short-distance region. Because of hard interaction at each QCD vertex one arrives at total helicity conservation in the process, the helicity flip amplitudes being suppressed by m_q^2/Q^2. This implies e.g. power suppression of the Dirac formfactor $F_2(Q^2)$ as compared to $G_M(Q^2)$, analogically the transition formfactor $G_{p\Delta}$ with helicity 3/2 is power suppressed as compared to that with helicity 1/2.

B. Elastic scattering

The outlined scheme can be applied to elastic scattering at large angles [14]. At fixed, large c.m. angle $\theta_{c.m.}$ and large Mandelstam variables s and t one can write the elastic amplitude for the process AB → CD in terms of the hadronic distribution amplitudes $\Phi_I(x, Q^2)$ and the hard scattering amplitude $M(x_i, s, t)$ (see Fig. 3a)

$$\mathcal{M}(s, t) = \int \prod_{i=a,b,c,d} \Phi_C^*(x_c, \tilde{p}_\perp)\Phi_D^*(x_d, \tilde{p}_\perp)M(x_i, s, t)\Phi_A(x_a, \tilde{p}_\perp)\Phi_B(x_b, \tilde{p}).$$

In leading order, $M(x_i, s, t)$ contains the sum of all connected valence quark diagrams. The external quark lines are nearly on shell and colinear with the corresponding initial and final hadrons (Fig. 3b). One easily sees that the number of possible amplitudes M is very large (e.g. in baryon-baryon scattering one finds about 10^4 different diagrams). This makes their exact computation very improbable. However one can still make some predictions

in particular concerning the power behaviour of the cross-section at fixed $\theta_{c.m.}$. All leading order amplitudes M fall as $\alpha_s(\alpha_s/s)^{n/2-2}$ where n is the total number of constituents in the initial and final states together. Knowing the behaviour of the distribution amplitudes, following from Eq. (2.3) one obtains [14]

$$\frac{d\sigma}{dt} \sim \left[\frac{\alpha_s(p_\perp^2)}{s}\right]^{n-2} \left(\ln \frac{p_\perp^2}{\Lambda^2}\right)^{-2\sum_{i=1}^{4}\gamma_i} \cdot f(\theta_{c.m.}), \tag{2.6}$$

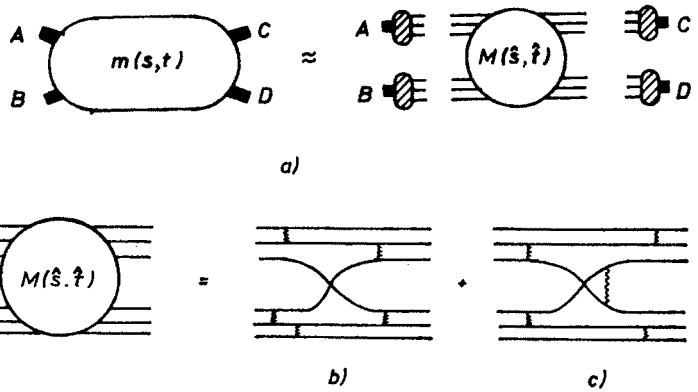

Fig. 3a) The decomposition of the elastic scattering amplitude; b) and c) The hard part of the elastic scattering diagram in leading order

where for mesons $\gamma_i = 0$ when their helicity $h = 0$ and $\gamma_i = -4/9(33-2n_f)$ when $|h| = 1$ and for baryons $\gamma_i = -2/9(33-2n_f)$ when $|h| = 1/2$ and $\gamma_i = -2/3(33-2n_f)$ when $|h| = 3/2$.

C. Spin effects in elastic scattering

The spin structure of elastic nucleon-nucleon scattering can be analyzed by looking at the polarization P and spin-spin asymmetries A_{ii}, $i = (n, l, s)$ (the independent helicity amplitudes Φ_i, $i = 1, \ldots, 5$ and the spin quantities P, A_{nn}, A_{ll}, A_{ss}, A_{sl} are defined in the Appendix A). The measurement of

$$A_{nn} = \frac{d\sigma/dt(\uparrow\uparrow)+d\sigma/dt(\downarrow\downarrow)-d\sigma/dt(\uparrow\downarrow)-d\sigma/dt(\downarrow\uparrow)}{d\sigma/dt(\uparrow\uparrow)+d\sigma/dt(\downarrow\downarrow)+d\sigma/dt(\uparrow\downarrow)+d\sigma/dt(\downarrow\uparrow)}$$

$$= \frac{2(\Phi_1^* \cdot \Phi_2 - \Phi_3 \cdot \Phi_4^*)}{|\Phi_1|^2+|\Phi_2|^2+|\Phi_3|^2+|\Phi_4|^2+4|\Phi_5|^2} \tag{2.7}$$

(spins of the initial protons projected perpendicular to the scattering plane) in $p_\uparrow p_\uparrow \to pp$ at large angles and $p_l = 11.75$ GeV/c ([6], see Fig. 4) caused some excitement when it turned out that at $\theta_{c.m.} = 90°$ protons with spins parallel scatter 4 times more often than with antiparallel spins. The calculation of the spin effects within lowest order QCD followed soon thereafter [15, 16]. The crucial point in both analyses is the helicity conservation

at each quark-gluon vertex. Taking into account the quark interchange diagrams of the type shown in Fig. 3b and summing all possible quark routings the nonzero unsymmetrized proton amplitudes are

$$\mathcal{M}_{++++}(s,t) = (N_{u+}^2 + N_{u-}^2 + N_{d+}^2 + N_{d-}^2)\cdot f(s,t) = \tfrac{31}{9} f(s,t)$$

$$\mathcal{M}_{+--+}(s,t) = (2N_{u+}N_{u-} + 2N_{d+}N_{d-}) f(s,t) = \tfrac{14}{9} f(s,t)$$

$$\mathcal{M}_{-++-}(s,t) = -((N_{u+} - N_{u-})^2 + (N_{d+} - N_{d-})^2) f(s,t) = -\tfrac{17}{9} f(s,t), \qquad (2.8)$$

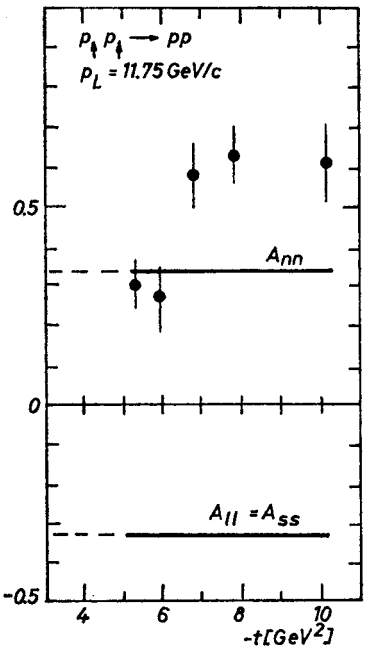

Fig. 4. The large angle data on A_{nn} at $p_L = 11.75$ GeV/c [6] together with the predictions of short distance diagrams [15, 16] on A_{nn} and A_{ll}

where $f(s,t)$ contains the colour and momentum dependent part of the amplitude and $N_{q\lambda}$ is the number of q-type quarks with helicity λ in the proton. Symmetrization of the amplitudes (2.8) leads to

$$\Phi_1(s,t) = \tfrac{1}{9}(31f(s,t) + 31f(s,u)),$$

$$\Phi_2(s,t) = 0$$

$$\Phi_3(s,t) = \tfrac{1}{9}(14f(s,t) + 17f(s,u)),$$

$$\Phi_4(s,t) = \tfrac{1}{9}(-17f(s,t) - 14f(s,u)),$$

$$\Phi_5(s,t) = 0. \qquad (2.9)$$

Analogous expressions for the np → np scattering are given in Appendix B.

Using (2.9) in Eqs (2.7) and (A.2) one obtains at 90°

$$A_{nn} = -A_{ll} = -A_{ss} = \tfrac{1}{3}. \tag{2.10}$$

The above values do not change by more than 2% when going to lower angles [15]. A characteristic feature of the quark interchange diagrams (Fig. 3b) is vanishing of Φ_2 due to helicity conservation and consequently

$$A_{nn} = -A_{ss}. \tag{2.11}$$

The predictions (2.10) are in disagreement with the pp experiment at 11.75 GeV/c (see Fig. 4). To cure them one can assume other important contributions to the amplitude at these energies and momentum transfers. The interference of the amplitudes (2.8) with instanton exchange diagrams [15] or pinch diagrams with σ-meson exchange [16] is able to increase the value of A_{nn}. However none of these two contributions is needed to describe any other effects in elastic scattering.

Not all QCD diagrams have been included in the above analysis. In particular the ones with the gluon exchange between the interchanged quarks (Fig. 3c) cannot be expressed with the same function $f(s, t)$ which was used in Eqs (2.8). The interference of these two types of diagrams can potentially increase the value of A_{nn}. A simple example of such mechanism is presented in Ref. [17]. However large value of the spin-spin asymmetry is there accidental and occurs only at energies close to 12 GeV/c.

3. Pinch diagrams in elastic scattering

An important contribution to elastic scattering was first noticed by Landshoff [2]. It occurs when all constituents in the initial hadrons have approximately equal light-cone momentum fractions x. In such configuration an on-shell scattering of all constituents with the exchange of equal momentum transfers is possible. Its power behaviour at fixed

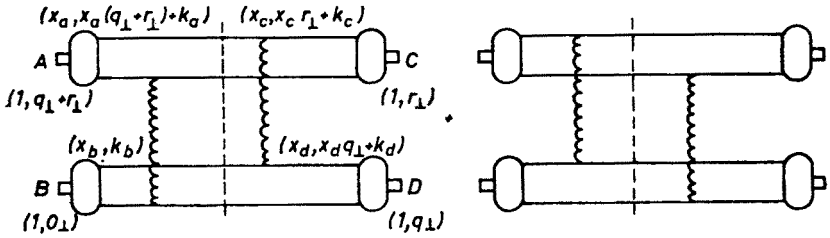

Fig. 5. The meson-meson scattering in the pinch region

c.m. scattering angle suggests the dominance of these diagrams over the ones governed by the dimensional counting rules [2].

We sketch the calculation in the case of meson-meson elastic scattering. The amplitude can be parametrized in the infinite momentum frame as in Fig. 5 [14]. Momentum conser-

vation gives then

$$x_a+x_b = x_c+x_d,$$

$$k_a+k_b-k_c-k_d = (x_c-x_a)r_\perp+(x_d-x_a)q_\perp.$$

In general the intrinsic transverse momenta k_i (i = a, b, c, d) are large. However for

$$(x_c-x_a) \leqslant \frac{\lambda}{r_\perp} \quad \text{and} \quad (x_d-x_a) \leqslant \frac{\lambda}{q_\perp}, \tag{3.1}$$

where λ is a scale characterizing soft interaction, all the transverse momenta inside the initial and final hadrons are small. Such a contribution is enhanced by the hadronic wave function which is peaked for small k_i. One can calculate the energy denominators connected with the diagrams of Fig. 5. (In fact they appear in the Feynman rules in the infinite momentum frame and light cone gauge [14].)

$$D_1 \approx (x_c-x_a)r_\perp^2+(x_d-x_a)q_\perp^2+2(\vec{k}_d-\vec{k}_a)\cdot\vec{q}_\perp+2(\vec{k}_c-\vec{k}_a)\cdot\vec{r}_\perp+O(\lambda^2)+i\varepsilon \tag{3.2}$$

$$D_{11} \approx -D_1^*+O(\lambda^2).$$

Adding the diagrams one obtains a δ function coming from the sum of the denominators

$$\frac{1}{D_1}+\frac{1}{D_{11}} = -2\pi i\delta(\Delta_c|r_\perp|+\Delta_d|q_\perp|),$$

where

$$\Delta_c \equiv (x_c-x_a)\,|r_\perp|+2(\vec{k}_{\perp c}-\vec{k}_{\perp a})\cdot\hat{r}_\perp$$

and

$$\Delta_d \equiv (x_d-x_a)\,|q_\perp|+2(\vec{k}_{\perp d}-\vec{k}_{\perp a})\cdot\hat{q}_\perp.$$

The scattering amplitude, proportional to

$$\mathcal{M}_{\pi\pi} \sim \int_0^1 dx_a dx_b dx_c dx_d \Psi_D^*(x_d)\Psi_C^*(x_c)\Psi_A(x_a)\Psi_B(x_b)$$

$$\times \frac{2\pi}{i} M_{qq}^2\delta(\Delta_c|r_\perp|+\Delta_d|q_\perp|)\delta(x_a+x_b-x_c-x_d)$$

$$= -\frac{4\pi i\lambda}{\sqrt{stu}}\int_0^1 dx_a \Psi_D^*(x_a)\Psi_C^*(x_a)\Psi_B(x_a)\Psi_A(x_a)M_{qq}^2(x_a, s, t)$$

where after the change of variables we integrated over Δ_c and Δ_d up to the scale λ.

Knowing the dimension of the quark-quark amplitude M_{qq} (in lowest order it is s^0) one

obtains

$$\frac{d\sigma}{dt} \sim \frac{\alpha_s^4(t)}{t^5} f(\theta_{c.m.})$$

which is one power less as compared to the prediction of the dimensional counting rules. Consequently this contribution may dominate the elastic scattering at highest energies and momentum transfers. Analogical derivation gives in the case of pp scattering

$$\frac{d\sigma}{dt} = A \frac{\alpha_s^6(t)}{t^8} f(\theta_{c.m.}). \tag{3.3}$$

In fact it is argued [18] that the function $f(\theta_{c.m.})$ is approximately a constant. One again sees that the cross-section (3.3) decreases slower at fixed $\theta_{c.m.}$ than the "dimensional counting rules" result $d\sigma/dt \sim 1/s^{10}$. The region where it dominates the cross-section depends

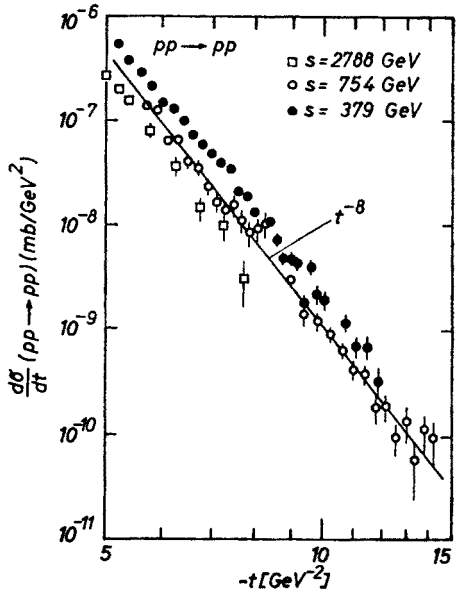

Fig. 6. $d\sigma/dt$ in pp elastic scattering at large t [19]. The curve represents $1/t^8$ behaviour [18]

on the exact value of the constant A. Its phenomenological estimate and comparison of Eq. (3.3) with the data [19] suggest that the region of 3 GeV^2 < $|t|$ ≪ s is well described by the pinch diagrams (see Fig. 6). This contribution, which is independent of energy at given t, is negligible then at large angles where $|t| \approx s$.

In the case of π N elastic scattering pure pinch singularity diagrams are not possible — at least one of the interacting quarks is far off-shell in the intermediate state. However hybrid diagrams [18] of the type shown in Fig. 7 give still dominant power behaviour ($d\sigma/dt \sim 1/t^7$).

From the above arguments one sees that the pinch singularity does not play any role in spin effects at large angles. For completeness we give however the resulting asymmetries in pp elastic scattering corresponding to the case with one gluon exchange in M_{qq} [20, 16]

$$A_{nn} = -A_{ss} = \tfrac{9}{41} \approx 0.22,$$

$$A_{ll} = -\tfrac{23}{41} \approx -0.56.$$

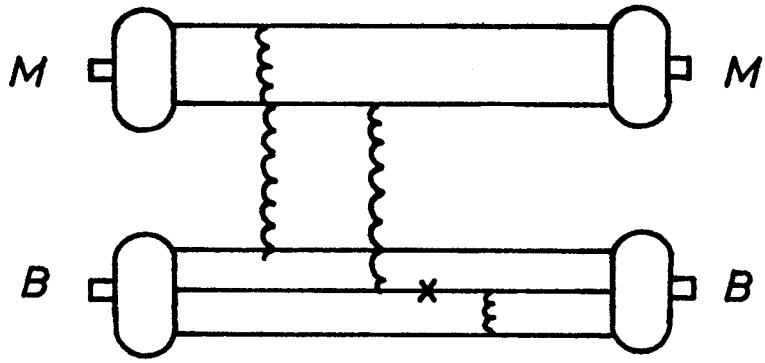

Fig. 7. The meson-baryon elastic scattering diagram in the pinch region [18]. The crossed line is far off shell

The smallness of A_{nn} is again due to helicity conservation at each vertex (only Φ_1, Φ_3 and Φ_4 are nonzero).

All the presented results are valid in the lowest order of perturbation calculation. Possible corrections are discussed in Section 5.

4. End-point contribution to exclusive processes

The idea of the end-point dominance in an elastic event was first suggested by Feynman [21] and was based on the assumption that the interacting parton carries almost all of the hadron momentum. In such a case the initial and final configurations were alike and consequently one obtained an elastic transition.

A quantitative formulation of this idea used to relate the behaviour of the formfactor at large Q^2, the structure function and the wave function at x close to 1 is known as the Drell-Yan-West relation [3]. We sketch their derivation for the meson formfactor in order to be able to use the same physical argument to extend the relations to elastic scattering.

It is assumed in this Section that the wave function at the end-point is dominated by soft effects.

A. The formfactor

The main idea in the end-point region is to keep the intrinsic transverse momenta of all constituents small, both in the initial and final state — such a contribution is enhanced by the soft wave function which is peaked at low $k_\perp$. Parametrizing the amplitude as in

Fig. 8 and making use of the momentum conservation the intrinsic transverse momenta for the upper quark line are $k_\perp$ and $(1-y)q_\perp+k_\perp = (1-x)q_\perp+k_\perp$ in the initial and final state respectively. Requiring both of them to be less than a scale λ, characterizing the soft process, below which there is no suppression of the above diagram by the wave function we obtain the condition

$$(1-x) < \frac{\lambda}{q} . \tag{4.1}$$

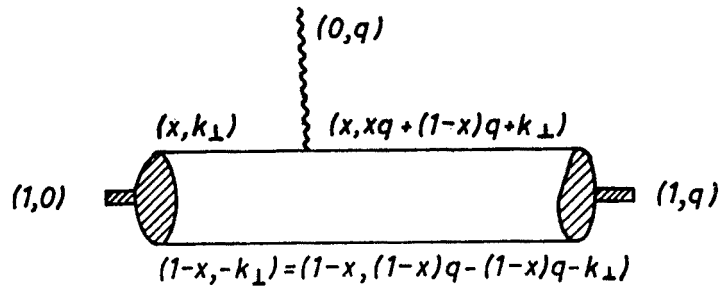

Fig. 8. The π formfactor in the end-point calculation

The formfactor is proportional to the overlap of the wave functions

$$F(Q^2) = \int dx dk_\perp \Psi^*(x, k_\perp+(1-x)q_\perp)\Psi(x, k_\perp). \tag{4.2}$$

One can make use of (4.1) in the integration of (4.2) over $k_\perp$ and the result does not depend on $q_\perp$, except of the integration limit

$$F(Q^2) \sim \int_{1-\frac{\lambda}{q_\perp}}^{1} dx|\Psi(x, \lambda)|^2.$$

The behaviour of the formfactor depends now on the tail of the soft wave function near $x = 1$. Similar calculation relates the structure function to the wave function at $x \to 1$. The Drell-Yan-West relations can thus be written in the following form:
If

$$\Psi(x, k_\perp) \sim (1-x)^\delta \quad \text{for} \quad x \to 1$$

then

$$F(Q^2) \sim (\lambda^2/Q^2)^{\delta+1/2} \quad \text{for} \quad Q^2 \to \infty$$

$$\nu W_2(x, Q^2) \sim (1-x)^{2\delta} \quad \text{for} \quad x \to 1. \tag{4.3}$$

The derivation of these relations for the baryons goes in a similar way with only slight modifications due to a greater number of constituents. The relations read in this case:

If

$$\Psi(x, k_\perp) \sim (1-x)^\delta \quad \text{for} \quad x \to 1$$

then

$$G_M(Q^2) \sim (\lambda^2/Q^2)^{\delta+1} \quad \text{for} \quad Q^2 \to \infty$$
$$\nu W_2(x, Q^2) \sim (1-x)^{1+2\delta} \quad \text{for} \quad x \to 1. \tag{4.4}$$

One notices that an appropriate choice of δ ($\delta = 1/2$ for the pion and 1 for the nucleon) leads to the agreement with the data. One also reproduces the "dimensional counting rules", however not from counting the dimensions of the calculated quantities but from the hadronic wave function which may be soft (for a recent analysis of the end-point contribution to elastic formfactor see Ref. [22]).

B. The elastic scattering — the Drell-Yan-West relations

The end-point dominance in elastic scattering is based on the same principle as in the formfactor calculation — small transverse momenta are required inside the hadrons [21]. This is obtained in the configuration where the constituents which exchange large momentum carry almost all the momentum of the hadrons. The remaining constituents with $x \approx 0$ are allowed to interact softly, this interaction however can be shifted to the hadronic wave function.

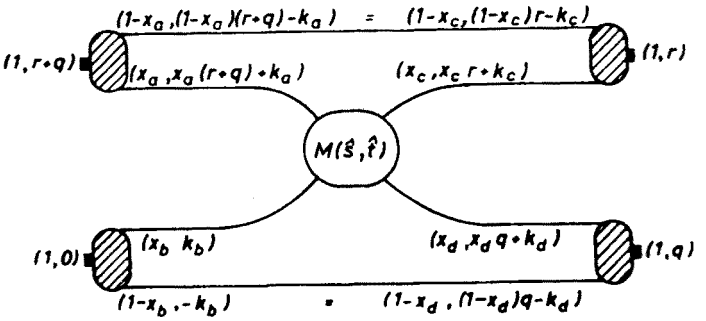

Fig. 9. The meson-meson elastic scattering in the end-point region

As a first example we calculate the meson-meson scattering amplitude. Assuming the valence quark dominance of the process the amplitude may be parametrized as in Fig. 9. There are two large variables in this process: $r_\perp$ and $q_\perp$, $r_\perp \cdot q_\perp = 0$. They are related to the Mandelstam variables by

$$s = r_\perp^2 + q_\perp^2, \quad t = -q_\perp^2, \quad u = -r_\perp^2.$$

Making use of the momentum conservation for the noninteracting lines we obtain

$$x_a = x_c = x,$$
$$y_b = y_d = y, \tag{4.5a}$$

$$(1-x)q_\perp = k_a - k_c,$$

$$(1-y)q_\perp = k_d - k_b. \tag{4.5b}$$

The equations (4.5b) mean that the intrinsic transverse momenta k_i (i = a, b, c, d) are small if

$$(1-y) \approx (1-x) < \frac{\lambda}{q_\perp}$$

a relation analogous to (4.1).

The scattering amplitude reads

$$\mathcal{M}(s,t) = \int dx dy dk_a dk_b \Psi_C^*(x, k_a + (1-x)q_\perp)\Psi_D^*(y, k_b + (1-y)q_\perp)$$

$$* M(x, y, r_\perp, q_\perp)\Psi_A(x, k_a)\Psi_B(y, k_b), \tag{4.6}$$

where $\Psi_i(x, k_\perp)$ is the wave function of the i-th meson, $M(x, y, r_\perp, q_\perp)$ — the fast quark scattering amplitude and we have made use of the momentum conservation. The integrals over the transverse momenta can be performed up to the scale λ which characterizes the soft interaction, this region being enhanced by the wave functions. The integral factorizes in this approximation and gives

$$\mathcal{M}(s,t) \sim \int_{1-\lambda/q_\perp}^{1} dx \Psi_C^*(x,\lambda)\Psi_A(x,\lambda) * \int_{1-\lambda/q_\perp}^{1} dy \Psi_D^*(y,\lambda)\Psi_B(y,\lambda)$$

$$* M(x \approx y \approx 1, s, t). \tag{4.7}$$

One recognizes the integrals as the meson formfactors, they coincide with those discussed before when A = C and B = D. The amplitude $M(1, 1, s, t)$ represents hard scattering of on-shell quarks. In this factorized part of the process one can use the dimensional counting rules [13]. They give the dimension of $M(1, 1, x, y)$ as (energy)^0. As a result the meson-meson amplitude $\mathcal{M}(s, t)$ behaves as follows

$$\mathcal{M}(s,t) \sim (\text{energy})^{-2-(\delta_A+\delta_B+\delta_C+\delta_D)}$$

up to logarithmic corrections. δ_I (I = A, B, C, D) is the power of the $(1-x)$ behaviour of the I-th wave function. The extension of the Drell-Yan-West relations to the case of elastic meson-meson scattering can be thus formulated in a following way:
If

$$\Psi_I(x, k_\perp) \sim (1-x)^{\delta_I} \quad \text{for} \quad x \to 1$$

then

$$\frac{d\sigma}{dt} \sim \left(\frac{1}{s}\right)^{4+\delta_A+\delta_B+\delta_C+\delta_D} f(\theta_{\text{c.m.}}) \quad \text{for large } s, t \text{ and } t/s \text{ fixed.} \tag{4.8}$$

Choosing in the case of $\pi\pi$ scattering δ_I as in Subsection A we obtain

$$\frac{d\sigma}{dt} \sim \left(\frac{1}{s}\right)^6 f(\theta_{\text{c.m.}}) \tag{4.9}$$

in agreement with the dimensional counting rules.

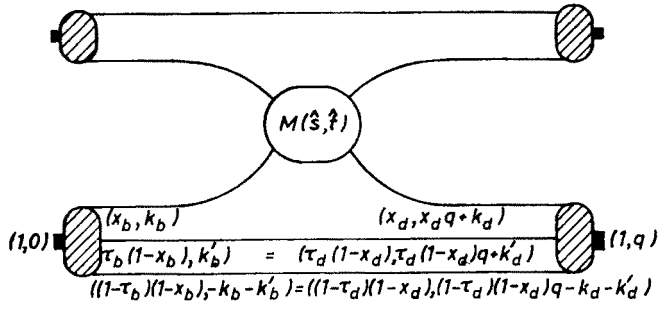

Fig. 10. The meson-baryon elastic scattering in the end-point region

To calculate the meson-baryon or baryon-baryon amplitude one proceeds along the same lines. The factorization occurs in analogy to Eq. (4.7) the baryonic vertex produces then (see Fig. 10)

$$\int dx_b(1-x_b) \int d\tau dk_\perp \Psi_D^+(x_b, \tau_b, k_b + (1-x)q_\perp)\Psi_B(x_b, \tau_b, k_b)$$

$$\sim \int_{1-\lambda/q_\perp}^{1} dx_b(1-x_b)\tilde{\Psi}_D^+(x_b, \lambda)\tilde{\Psi}_B(x_b, \lambda), \tag{4.10}$$

where

$$\tilde{\Psi}_D^+(x_b, \lambda)\tilde{\Psi}_B(x_b, \lambda) = \int_0^1 d\tau_b \Psi_D^+(x_b, \tau_b, \lambda)\Psi_B(x_b, \tau_b, \lambda).$$

We recognize the baryon formfactor in this expression. The Drell-Yan-West relations extended to this case look as follows:

Meson-baryon scattering (A,C-mesons, B,D-baryons):

$$\frac{d\sigma}{dt} \sim \left(\frac{1}{s}\right)^{5+\delta_A+\delta_B+\delta_C+\delta_D} f(\theta_{\text{c.m.}}). \tag{4.11}$$

With the previous choice for δ_I

$$\frac{d\sigma}{dt} \sim \left(\frac{1}{s}\right)^8 f(\theta_{\text{c.m.}}). \tag{4.12}$$

Baryon-baryon scattering

$$\frac{d\sigma}{dt} \sim \left(\frac{1}{s}\right)^{6+\delta_A+\delta_B+\delta_C+\delta_D} f(\theta_{\text{c.m.}}) \tag{4.13}$$

with δ_I fixed before ($\delta_I = 1$)

$$\frac{d\sigma}{dt} \sim \left(\frac{1}{s}\right)^{10} \cdot f(\theta_{\text{c.m.}}) \tag{4.14}$$

Both results (4.12) and (4.14) coincide with the dimensional counting rules. However we stress once again that they do not follow from the hard subprocess but depend crucially on the behaviour of the hadronic wave function.

One problem is new when extending the Drell-Yan-West relations to elastic scattering. One is dealing in the present case with two variables $r_\perp$ and $q_\perp$, both of them being large. In the large angle region where $r_\perp/q_\perp = \varrho \approx 1$ both conditions $(1-x) \leqslant \lambda/q_\perp$ and $(1-x) \leqslant \lambda/r_\perp$ assure small intrinsic transverse momenta. Consequently one is facing the problem, which of the two variables determines the integration limits in Eqs (4.7) and (4.10) or in other words, what are the arguments of the formfactors which appear in these expressions.

C. Elastic scattering — the differential cross-section

Very simple form of the amplitude in the end-point region allows its explicit calculation, at least in the leading order.

We begin with the nucleon-nucleon elastic scattering where the amplitude can be tested with respect to its energy and angular dependence or its flavour and crossing properties. The hadronic amplitude $\mathcal{M}(s, t)$ is related to the hard, on-shell quark-quark scattering amplitude $M(\hat{s}, \hat{t})$ with $\hat{s} = \langle x\rangle \cdot \langle y\rangle \cdot s \approx s$ and $\hat{t} = \langle x\rangle \cdot \langle y\rangle \cdot t \approx t$. In leading order

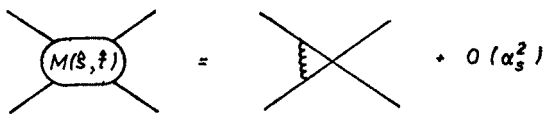

Fig. 11. The hard part of elastic scattering diagram in leading order

$M(s, t)$ contains one gluon exchange, with interchanged legs (see Fig. 11) to allow for colour singlet exchange in the t-channel. It is interesting to notice that the simple quark interchange diagrams (without interaction), typical for the Constituent Interchange Model [23], do not contribute to the end-point singularity.

The two independent quark amplitudes are in leading order

$$M_{++++}(s, t) = 4\pi\alpha_s \frac{s}{u}, \qquad M_{-++-}(s, t) = 4\pi\alpha_s \frac{t}{u}, \tag{4.15}$$

where the indices $\pm$ denote the quark helicities.

The mentioned problem of the proper choice of the formfactor arguments can be solved by noticing that a single diagram (before t-u symmetrization) is approximately t-u symmetric in the limit $\alpha_s \to 0$. The general form of $\mathcal{M}(s, t)$ is thus

$$\mathcal{M}(s, t) = G_M(t)G_M(u)M(s, t).$$

It reminds of models [24] used for a long time in elastic scattering, in our case however the formfactors have different arguments and the form of the quark-quark amplitude is strictly defined.

The exact expression for $\mathcal{M}(s, t)$ depends on the spin configuration of the nucleons and combinatorical factors following from different ways of interchanging quark lines [25]. In the case of pp scattering the amplitudes read:

$$\mathcal{M}_{++++}(s,t) = \tfrac{1}{9}[31M_{++++}(s,t)+14M_{+--+}(s,t)]G_M(t)G_M(u),$$

$$\mathcal{M}_{++--}(s,t) = \tfrac{1}{9}[17M_{++--}(s,t)]G_M(t)G_M(u),$$

$$\mathcal{M}_{+-+-}(s,t) = \tfrac{1}{9}[31M_{+-+-}(s,t)+14M_{++++}(s,t)]G_M(t)G_M(u),$$

$$\mathcal{M}_{-++-}(s,t) = \tfrac{1}{9}[17M_{-++-}(s,t)]G_M(t)G_M(u),$$

$$\mathcal{M}_{+++-}(s,t) = 0. \tag{4.16}$$

The remaining amplitudes are related to the above ones due to parity conservation, time reversal invariance and identical particle relations (see Appendix A). The appropriate t-u symmetrization completes the construction of the PP scattering amplitudes (see Appendix A). The spin structure of Eqs (4.16) is discussed in more detail in the next subsection. For the nucleon formfactor we take the standard dipole form.

The resulting curves for the differential cross-section $d\sigma/dt$ as a function of t for $s = 28.6$, 33.5, 37.8 and 41.8 GeV^2 and $|t| \geqslant 5$ GeV^2 are shown in Fig. 12. The large angle

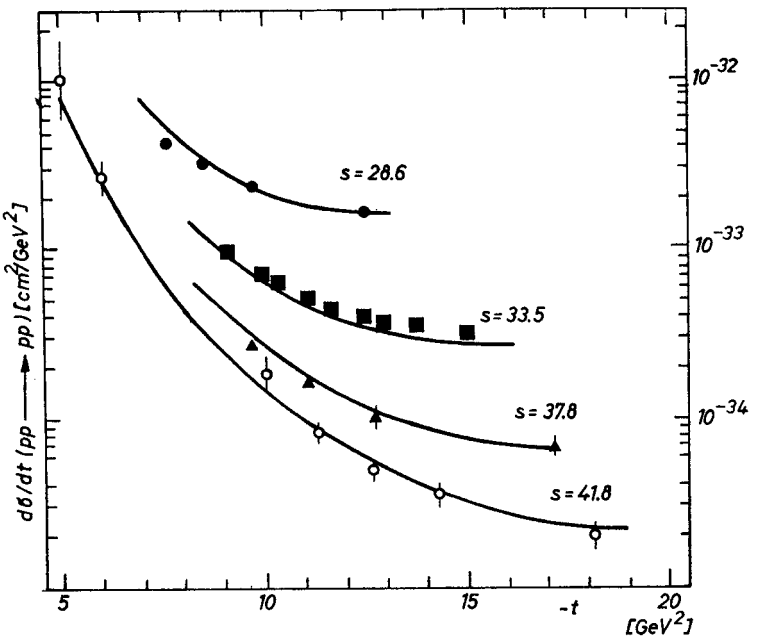

Fig. 12. $d\sigma/dt$ of pp elastic scattering at large angles [26] together with the end-point prediction

data [26] at these energies are also plotted showing very good agreement with the calculated cross-section. The only free parameter is the overall normalization. It can be expressed through the strong coupling constant α_s which is kept fixed. Its estimate gives too large value of α_s suggesting a possibility of additional soft interaction among the hadrons [27]. It may be particularly important in the end-point region where even some of the valence quarks have $x \approx 0$, but is expected to influence only the normalization of the process.

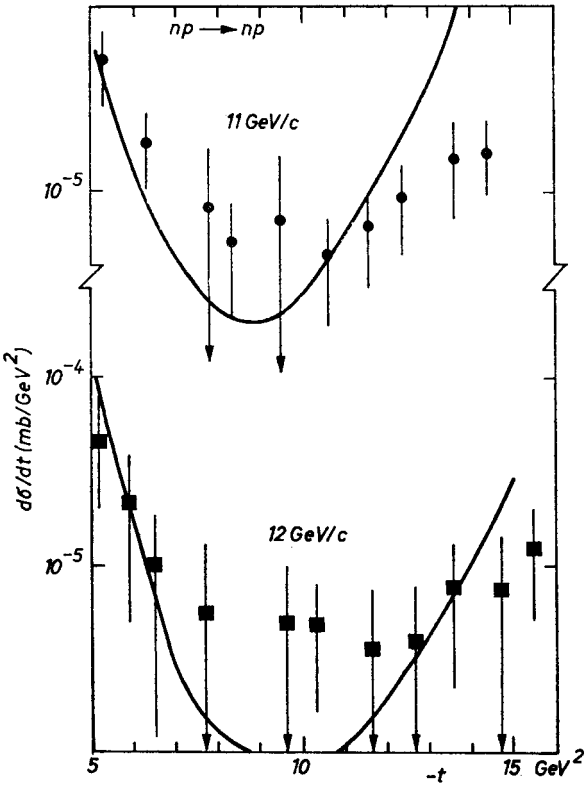

Fig. 13. The same as in Fig. 12 but for np elastic scattering

Having the full shape of the proton-proton amplitude including its fixed normalization, we can test its flavour and crossing properties. The neutron-proton scattering amplitudes are obtained by interchanging u and d quarks in one of the nucleons. The resulting amplitudes are given in Appendix B. Their comparison with the 11 and 12 GeV/c np data [28] shows good agreement (see Fig. 13).

The $\bar{p}p$ amplitudes are obtained by crossing which means in this case the interchange of the Mandelstam variables s and u. Again the agreement with the data [29] is very good (see Fig. 14).

The meson-nucleon scattering can be treated in full analogy. One important change occurs here only in the choice of the arguments of the formfactors. The previously used

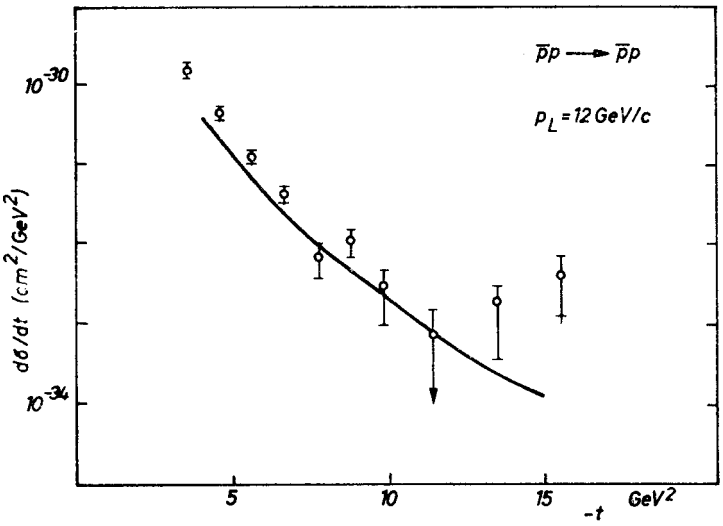

Fig. 14. The same as in Fig. 12 but for $\bar{p}p$ elastic scattering

argument does not hold in this case and we chose t as the variable in both formfactors. (For the π formfactor a simple $1/|t|$ form is assumed). The amplitudes read as follows

$$\mathcal{M}_{++}(s,t) = \tfrac{1}{2}\left[2M^{u}_{++++}(s,t)+2M^{u}_{+--+}(s,t)+M^{d}_{++++}(s,t)+M^{d}_{+--+}(s,t)\right]G_M(t)F_\pi(t)$$

$$\mathcal{M}_{+-}(s,t) = \tfrac{1}{6}\left[8M^{u}_{+++-}(s,t)-M^{d}_{+++-}(s,t)\right]G_M(t)F_\pi(t)$$

with the nonzero quark helicity amplitudes

$$M^{u}_{++++}(s,t) = 4\pi\alpha_s\frac{s}{u}$$

$$M^{d}_{+--+}(s,t) = 4\pi\alpha_s\frac{u}{s}$$

in the case of $\pi^+p \to \pi^+p$ and

$$M^{u}_{+--+}(s,t) = 4\pi\alpha_s\frac{u}{s}$$

$$M^{d}_{++++}(s,t) = 4\pi\alpha_s\frac{s}{u}$$

in the case of $\pi^-p \to \pi^-p$. We present $d\sigma/dt$ together with the large angle data [30] in Fig. 15.

Other exclusive processes (e.g. $\pi^-p \to \pi^0n$, $pp \to p\Delta$) can be analyzed easily along the same lines.

The agreement of the derived end-point contribution is remarkable. It is obtained with a special choice of the powers δ_I which leads to dimensional counting rules. In lowest order their modification is only by α_s^2, too gentle to be detected in quantities with high powerlike behaviour. On the other hand the short distance amplitudes of Section 2 go with

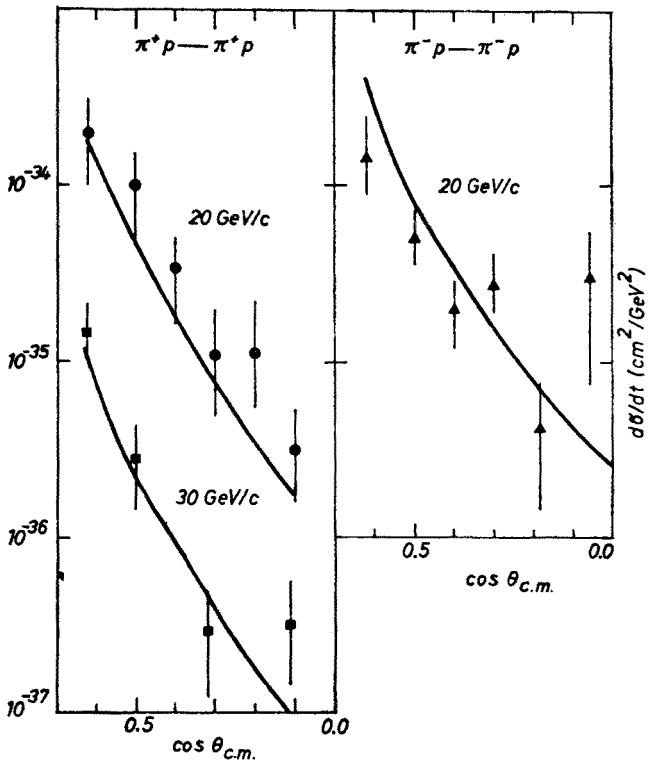

Fig. 15. The same as in Fig. 12 but for $\pi^{\pm}$p elastic scattering

the same power of energy. Although the QCD logarithmic modification is much stronger there and it is possible that the phenomenological success of this contribution may be destroyed, there is no way to tell which of these two terms dominates at present energies unless the unknown function of c.m. angle in Eq. (2.6) is calculated.

To solve this problem we advocate for the investigation of spin effects in elastic scattering.

D. Spin effects in the elastic scattering [31]

The end-point region requires special treatment when the spin is taken into account. We are not allowed to assume the s-channel helicity conservation at each vertex in the situation when only part of the process is hard. In particular in the interaction among the slow quark lines the ratio of the effective mass to the energy of the subprocess may be quite large.

The most important step consists in the impulse approximation. The hard process which is factorized and builds up $M(s, t)$ is short on the time scale as compared to the soft interaction within the single nucleon. One can therefore cut out the hard part of the nucleon amplitude (as in Fig. 16) and calculate easily its spin structure (s-channel helicity conserva-

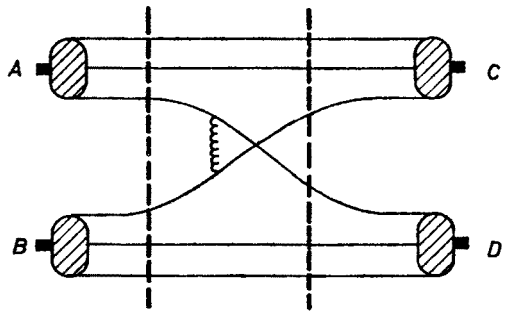

Fig. 16. The impulse approximation in the end-point region. The cut-out part of the elastic amplitude is short on time scale

tion in $M(s, t)$). The quarks which do not interact in the cut out diagram propagate freely and conserve their spin projections. To make both these conditions consistent one has to assume the helicity conservation in a frame where these quarks move along straight lines. The construction of the amplitude consists thus of the following steps:

— take the known quark helicity amplitudes $M(s, t)$ (Eqs (4.15))

— rotate them to the frame (called the Gottfried-Jackson frame [32]) where the spectator quarks move along straight lines

$$M^{\mathrm{GJ}}_{\gamma\delta\alpha\beta}(s, t) = \sum_{\substack{\alpha'\beta' \\ \gamma'\delta'}} d^{1/2}_{\alpha\alpha'}(\theta^{\mathrm{a}}_{\mathrm{GJ}}) d^{1/2}_{\beta\beta'}(\theta^{\mathrm{b}}_{\mathrm{GJ}}) d^{1/2}_{\gamma\gamma'}(0^{\mathrm{c}}_{\mathrm{GJ}}) d^{1/2}_{\delta\delta'}(\theta^{\mathrm{d}}_{\mathrm{GJ}}) M_{\gamma'\delta'\alpha'\beta'}(s, t).$$

The angles θ^{i}_{GJ} are fixed by the kinematics and the nucleon mass m_{N} [33]

$$\cos\theta_{\mathrm{GJ}} = \pm\sqrt{\frac{st}{(s-4m_{\mathrm{N}}^2)(t-4m_{\mathrm{N}}^2)}}. \tag{4.18}$$

The upper (lower) sign holds for the initial (final) particles. These angles are plotted on the velocity diagram in Fig. 17

— relate the nucleon amplitudes $\mathcal{M}_{\gamma\delta\alpha\beta}(s, t)$ to the quark amplitudes $M_{\gamma\delta\alpha\beta}(s, t)$ via Eqs (4.16). This step can be done only in the Gottfried-Jackson frame where we are sure that the noninteracting quarks do not influence the nucleon spin structure. One sees that Gottfried-Jackson frame is a spin system where the helicity and z-spin conservation mean the same. It was extensively used in low $p_{\perp}$ scattering [34].

The above construction is complete and does not introduce any free parameters. After performing it one can look what is the form of the s-channel helicity amplitudes.

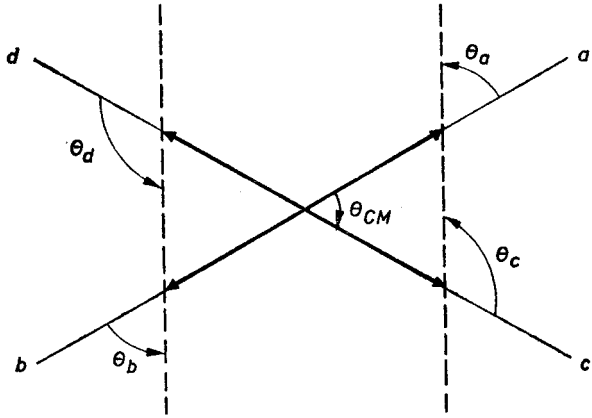

Fig. 17. The Gottfried-Jackson angles on the velocity diagram of elastic scattering

(To obtain them one needs to perform another rotation of the spin quantization axis by the angles $-\theta_i$). In the case of proton-proton scattering their unsymmetrized form reads:

$$\mathcal{M}_{++++}(s,t) = \tfrac{1}{9}[(17+b(s,t))M_{++++}(s,t)+c(s,t)\cdot M_{-++-}(s,t)]G_M(t)G_M(u)$$

$$\mathcal{M}_{++--}(s,t) = \tfrac{1}{9}[-c(s,t)M_{++++}(s,t)+(-14+d(s,t))M_{-++-}(s,t)]G_M(t)G_M(u)$$

$$\mathcal{M}_{+-+-}(s,t) = \tfrac{1}{9}[b(s,t)M_{++++}(s,t)+c(s,t)M_{-++-}(s,t)]G_M(t)G_M(u)$$

$$\mathcal{M}_{-++-}(s,t) = \tfrac{1}{9}[c(s,t)M_{++++}(s,t)+(31-d(s,t))M_{-++-}(s,t)]G_M(t)G_M(u)$$

$$\mathcal{M}_{+++-}(s,t) = 0$$

$$b(s,t) = 14-24\cos^2\theta_{GJ}+10\cos^4\theta_{GJ}$$

$$c(s,t) = -10\cos^2\theta_{GJ}\sin^2\theta_{GJ}$$

$$d(s,t) = 14-4\cos^2\theta_{GJ}-10\cos^4\theta_{GJ}. \qquad (4.19)$$

The detailed treatment of spin does not influence the differential cross section. It is however crucial for the spin-spin asymmetries. The predicted curves at $p_L = 11.75$ GeV/c are shown in Fig. 18. The relation $A_{nn} = -A_{ss}$ is badly broken due to $\Phi_2 \neq 0$. This is also the reason for large value of A_{nn} at high momentum transfers. The effect is explicitly seen when using the quark transversity amplitudes $N_{\gamma\delta\alpha\beta}$ [35]. In this representation both the spectator and interacting quarks conserve their transversities (the spin projections perpendicular to the scattering plane). If the nucleons have parallel transversities only quarks with parallel transversities can interact (only $N_{++++} \neq 0$) otherwise a state with spin 3/2 is produced. If, however, the nucleons have opposite transversities both N_{++++} and N_{--++} contribute. Their interference in the nucleon amplitude depend on the frame in which they are related to the nucleon amplitudes or, in other words, in which the impulse approximation is assumed. In the Gottfried-Jackson frame they nearly cancel. This causes the scattering

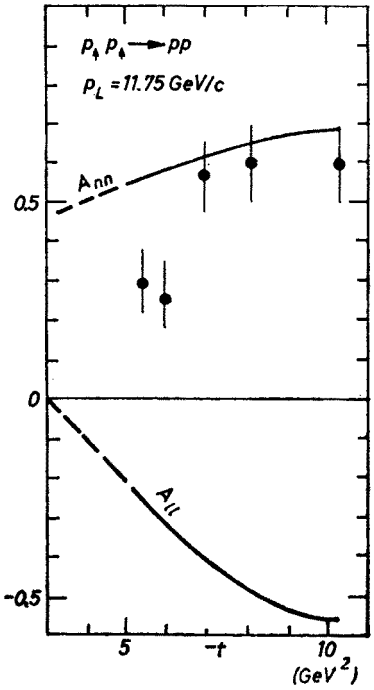

Fig. 18. The large angle data on A_{nn} at $p_L = 11.75$ GeV/c in pp elastic scattering [6] together with the end-point prediction on A_{nn}, A_{ll} and A_{ss}

of protons with antiparallel transversities much weaker than that with parallel transversities.

The results of similar analysis applied to np-elastic scattering are shown in Fig. 19. The corresponding formulae are given in Appendix B.

As a final remark we stress once more the role of the spin asymmetries. Their predicted values differ significantly in the short-distance and end-point regions making a clear distinction possible. The measured values of A_{nn} support the dominance of the end-point diagrams at momentum transfers around 10 GeV^2. This mechanism predicts $A_{nn}(90°)$ to stay around the present value as the energy increases (e.g. at $p_L = 26$ GeV/c $A_{nn}(90°) = 0.7$).

The above analysis may be improved when another spin-spin asymmetry is aviable. In particular the measurement of A_{ll} at $p_L = 11.75$ GeV/c, of which preliminary results already exist [36], can be very helpful in solving the problem of helicity conservation.

E. The nucleon wave function from exclusive and inclusive spin effects

In the preceding sections the nucleon wave function was assumed to be SU(6) spin-flavour symmetric. For example the form of the spin-flavour part of the proton wave function with the spin in + direction reads [37]

$$\Psi^p_+ = \frac{1}{\sqrt{18}}[2S(u_+u_+d_-) - S(u_+u_-d_+)] \tag{4.20}$$

with S being totally symmetric under permutations. If we select the quark which undergoes hard scattering in the end-point region, the remaining quarks (the spectator diquark) can be in spin 0 or 1 state. The later one is particularly important for the procedure described in the proceeding subsection. If the spectators had been always in $S = 0$ state, we could have related the quark amplitudes to the nucleon ones in any spin frame and the asymmetries would have been asymptotically $A_{nn} = 1/9$, $A_{ll} = -7/9$, $A_{ss} = -1/9$ as in the case of electron-electron elastic scattering.

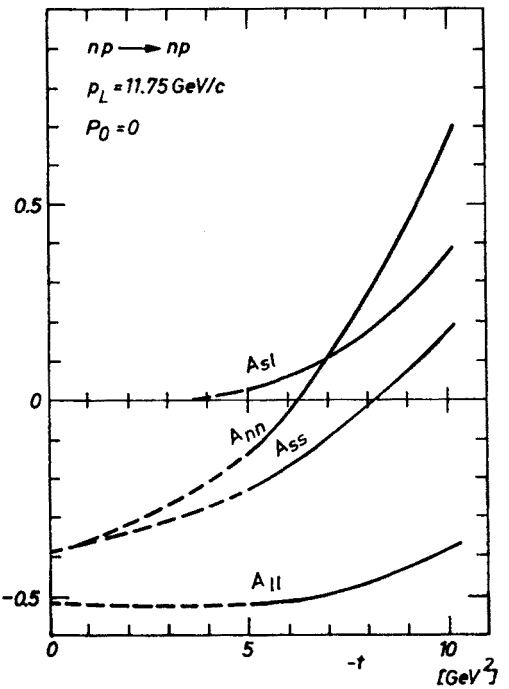

Fig. 19. The end-point predictions on A_{nn}, A_{ll} and A_{ss} in np elastic scattering at $p_L = 11.75$ GeV/c

The information on the nucleon wave function is also contained in the deep inelastic processes. The data [38–40] on these reactions seem to suggest the violation of the SU(6) symmetry, especially at x close to 1. Some models assume that there is no term with $S = 1$ diquark at $x = 1$, a disaster for the exclusive spin-spin asymmetries!

The problem of this subsection is to check the consistency of the exclusive and inclusive spin effects and display the limits put on the nucleon wave function by these phenomena. The analysis assumes that the spin effects in deep inelastic scattering are caused by the SU(6) symmetry breaking. We are aware of other possible explanations [41], in such cases the results of the previous subsection do not change and the analysis below does not apply.

In the model [42], which accounts for most of the deep inelastic spin phenomena

at $x \to 1$, one writes the proton structure function

$$F_2^p(x) = \tfrac{4}{9} A_0(x) + \tfrac{2}{9} A_1(x)$$

where $A_s(x)$ denotes the contribution in which the noninteracting quarks are in spin and isospin state s. The SU(6) symmetry means $A_0(x) = A_1(x)$. Following the arguments [43] from the Regge behaviour at $x \approx 0$ the model assumes

$$A_1(x) = a(1-x)A_0(x) \tag{4.21}$$

with a estimated around 3/2. Its predictions for the ratio of the neutron to proton structure functions F_2^n/F_2^p, the ratio of the down to up quarks in the proton d/u and the photon-proton asymmetry $A^{\gamma p} = \dfrac{\sigma^{1/2} - \sigma^{3/2}}{\sigma^{1/2} + \sigma^{3/2}}$ (σ^λ denotes the γp cross-section with total helicity λ) can be easily obtained

$$\frac{F_2^n(x)}{F_2^p(x)} = \frac{1+3a(1-x)}{4+2a(1-x)},$$

$$\frac{d(x)}{u(x)} = \frac{2a(1-x)}{3+a(1-x)},$$

$$A^{\gamma p} = \frac{6-a(1-x)}{6+3a(1-x)}.$$

They agree very well with the existing data [38–40] for large x (see Fig. 20). (Only the valence quarks are included, so we do not attempt to describe the whole x range).

Our problem is to translate the information contained in the above model for the behaviour of the nucleon wave function which is used to calculate the elastic spin-spin asymmetries.

The spin + proton wave function (Eq. (4.20)) can be written in an alternative form:

$$\Psi_+^p = \frac{1}{\sqrt{54}} [\sqrt{27}\, B_0^{u+} + \sqrt{12}\, B_1^{d-} + \sqrt{3}\, B_1^{u+} - \sqrt{6}\, B_1^{u-} - \sqrt{6}\, B_1^{d+}]. \tag{4.22}$$

The quark which undergoes scattering is explicitly written, together with its spin projection. The lower index stands for the spin (and isospin) of the spectator diquark. Each B_s^q is separately normalized. Remembering that $A_s(x)$ is proportional to the square of the diquark wave function Eq. (4.21) means

$$B_0^q(x) = B_1(x) + \gamma(x)\tilde{B}_0(x) \tag{4.23}$$

with

$$\gamma(x) = \sqrt{-1 + \frac{1}{a(1-x)}}. \tag{4.24}$$

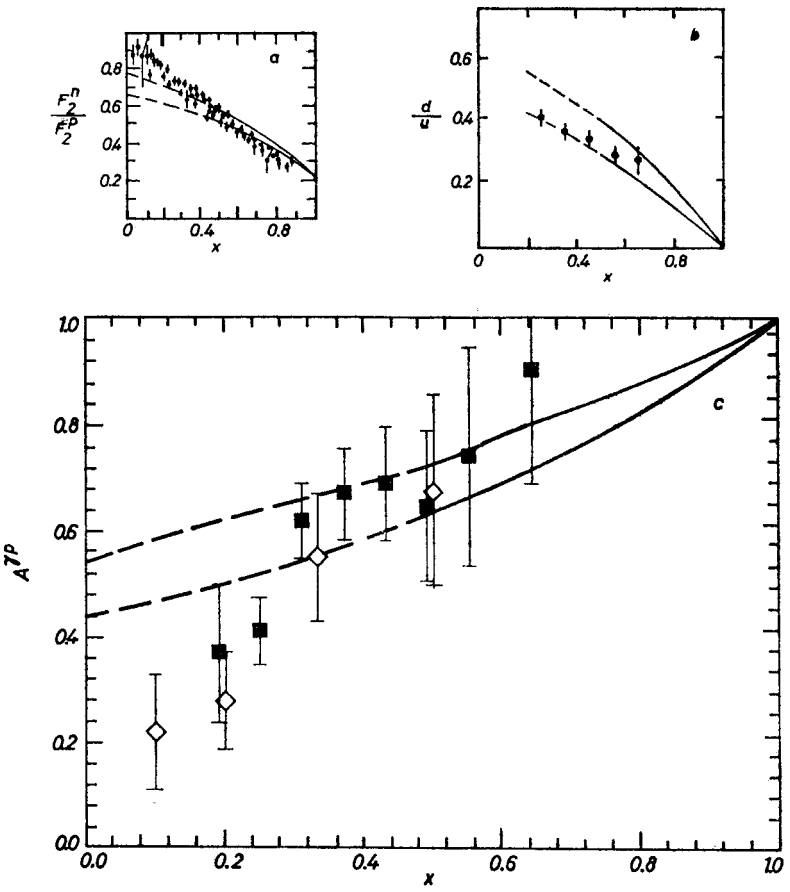

Fig. 20. The data on a) the ratio of neutron to proton structure functions $F_2^n(x)/F_2^p(x)$ [38]; b) the ratio of the down to up quarks in the proton $d(x)/u(x)$ [39]; c) the asymmetry $A^{\gamma p}(x)$ [40] compared with the predictions of the Carlitz-Kaur model [42]

$B_0(x)$ and $B_1(x)$ are the same functions of x, $\gamma \cdot B_0$ being the SU(6) symmetry breaking term. They are assumed not to interfere. Substituting (4.23) into (4.22) we obtain

$$\Psi_+^p = \frac{1}{\sqrt{6(9+4\gamma^2)}}(\sqrt{27}\, B_1^{u+} + \sqrt{12}\, B_1^{d-} + \sqrt{3}\, B_1^{u+} - \sqrt{6}\, B_1^{u-} - \sqrt{6}\, B_1^{u+})$$

$$+ \frac{\gamma}{\sqrt{6(9+4\gamma^2)}} \sqrt{24}\, \tilde{B}_0^{u+}. \tag{4.25}$$

The wave function (4.25) is of the form

$$\Psi^p = \sqrt{1-\beta^2}\, \Psi^{SU(6)} + \beta \Psi^{\overline{SU(6)}}.$$

The first term represents the SU(6) symmetric and the second — SU(6) breaking term, with

$$\beta(x) = \sqrt{\frac{1-a(1-x)}{1+a(1-x)}}. \tag{4.26}$$

The shape of the wave function (4.25) with $\beta(x)$ given by (4.26) can now be implemented in the calculation of the spin-spin asymmetries. The important point is that the end-point region defined by Eq. (4.1) is still quite broad at present momentum transfers (for $t \approx -10\ \mathrm{GeV}^2$ $x \geqslant 1-\lambda/\sqrt{-t} \approx 0.7$). Assuming that the average x is somewhere in the allowed region ($x \in (0.7, 0.9)$) we give in Fig. 21 the predictions for the range in which A_{nn}

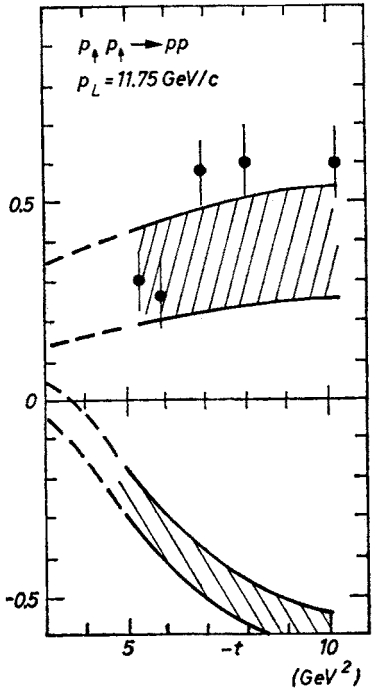

Fig. 21. The end-point prediction on A_{ll} and A_{nn} at $p_L = 11.75$ GeV/c with SU(6) symmetry breaking in the wave function. The data [6] on A_{nn} are also shown

and A_{ll} change. It is seen that the proposed form of the wave function (Eq. (4.25)) is compatible with both exclusive and inclusive measurements. The prediction concerning A_{nn} at higher momentum transfer changes however as compared to that from the previous subsection in the case when the above SU(6) symmetry breaking occurs. A_{nn} is supposed to decrease with t as x approaches 1.

One final remark should be added: the behaviour of the wave function at x close to 1 is assumed to be due to soft effects. Other approaches [44], which calculate this tail of the wave function perturbatively have problems with spin-spin asymmetries as mentioned in Section 2. They are nevertheless compatible with the deep inelastic data [45].

5. *Higher order corrections to exclusive processes*

In this section we review the main results, more details can be found e.g. in Ref. [46, 47].

As already mentioned higher order corrections are fully under control in the meson formfactor calculation. This means that one is able to disentangle the hard and soft regions of the amplitude and write it in a factorized form or, in other words, to use the Wilson [48] operator product expansion for this process. Moreover the factorized hard part ("coefficient function") obeys the renormalization group equation (RGE). These two conditions assure that the Sudakov effects [49] are cancelled in an exclusive process. The effect can be seen at each order of perturbation expansion, for example in the second order calculation of the π formfactor the Sudakov formfactor diagrams (Fig. 22a) are cancelled by the gluon exchange diagrams (Fig. 22b). This occurs only for colour singlet

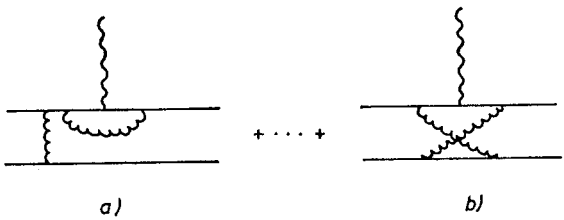

Fig. 22a) An example of the Sudakov type diagram in second order calculation of the π formfactor; b) an example of second order diagrams which cancel the diagrams of a)

states and far from the end-point region because the exchanged gluons transfer non--negligible longitudinal momentum. Consequently the end-point contribution is expected to be suppressed in higher orders by the Sudakov formfactor

The situation is less clear in the baryon formfactor. Double flow diagrams of the type shown in Fig. 23a lead to the failure of the renormalization group equation in this case. Although these diagrams turn out to be suppressed when Sudakov effects (Fig. 23b) are included, it has not been shown up to now that RGE is restored after taking into account all diagrams.

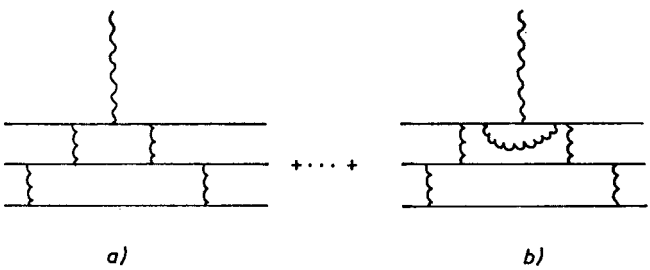

Fig. 23a) A double flow diagram in baryon formfactor calculation which leads to the failure of the RGE; b) a Sudakov type diagram which suppresses diagrams of a)

The situation is even less clear in wide angle elastic scattering. The potentially dominant pinch diagrams, discussed in Section 3, obtain a Sudakov type factor [50]

$$\exp\left[-\frac{24C_F}{33-2n_f}\left|\ln s(\ln\ln s-\ln Xs)-\ln\frac{1}{X}\right|\right], \tag{5.1}$$

where $X = O\left(\frac{1}{s}\right)$. Similarly it seems to happen to the end point region. The exact behaviour at finite energy depends however on the scale put in the Sudakov factors (5.1) and the magnitude of the soft wave function which normalizes each of the contributions in a different way.

Some information concerning the scale and the range of perturbative region can be obtained from the second order corrections to the hard part of the π formfactor [51]. The problem to be solved here is the choice of the right variable in the argument of α_s. It should be the average virtuality of internal lines divided by Λ_{QCD}, e.g. in the diagram of Fig. 24

$$k^2/\Lambda^2_{QCD} \approx \langle x\rangle\,\langle x'\rangle Q^2/\Lambda^2_{QCD}. \tag{5.2}$$

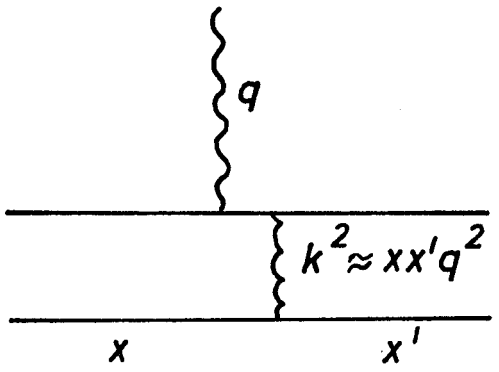

Fig. 24. A leading order hard diagram in π formfactor calculation

Proceeding in the standard way, i.e. minimizing the correction, and additionally taking Λ_{QCD} from other estimates one is able to learn what is the argument of the strong coupling constant at given Q^2. It turns out [51] that with currently accepted value of $\Lambda_{QCD} = 0.2$ GeV the variable $\langle k^2\rangle = 1$ for $Q^2 \approx 200$ GeV^2. This means that for $Q^2 < 200$ GeV^2 one is not allowed to use perturbation calculation! From Eq. (5.2) one immediately sees that the quark lines not hit by the photon are relatively slow ($x \leqslant 0.07$). This is due to rather broad π wave function and logarithmic singularities in the second order hard diagrams. One concludes, that even starting with perturbative methods, the process turns out to be deeply in the non-perturbative end-point region at presently accessible Q^2.

6. Spin effects in the inclusive production — baryon polarization at large transverse momentum

Baryon polarization in the inclusive production at large energies has been studied extensively in the last few years. The measurement [7] of hyperon polarization which increases with the transverse momentum (see Fig. 25) seemed to be a surprise — at high momentum transfer one would expect a real, hard amplitude to dominate and consequently negligible polarization.

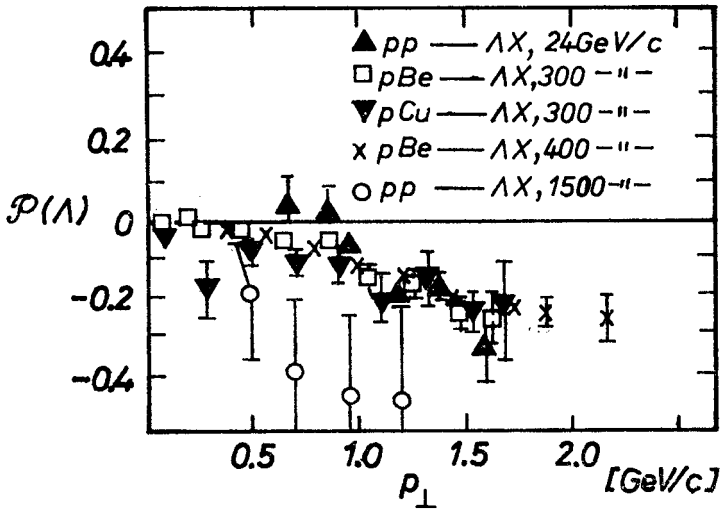

Fig. 25. The Λ polarization in inclusive production as a function of transverse momentum [7]

A. The multiple quark scattering model [52]

In this subsection we present a single idea which explains the observed features of baryon polarization. From the presented arguments it follows that the data are rather in an intermediate region of transverse momentum and one is not allowed to use the hard scattering technique. Therefore no attempt is made to give a quantitative description — it would have been, to our experience, very model dependent.

Let us start with the Λ production in nucleon induced reactions. The SU(6) symmetric Λ wave function consists of the ud diquark in the spin-isospin state $S = I = 0$ and the strange quark s. Consequently the spin projection of the Λ is entirely given by the spin projection of the s-quark and the Λ polarization equals the s-quark polarization. Looking into the proton hemisphere one already has a $\mathrm{ud}|_{S=I=0}$ system coming from the proton valence quarks. During the collision the s-quark, which may originate from the proton sea or be produced in a subprocess $g \to s\bar{s}$, becomes a valence quark and recombines to Λ. In both cases its energy in the c.m. system is low. The energy is thus given essentially by the ud-diquark energy.

Both the $q_\perp$ of the diquark and $k_\perp$ of the s-quark contribute to the transverse momentum $p_\perp$ of the Λ. Looking for the Λ with a given $p_\perp$ one chooses in most cases a configuration where the $k_\perp$ points in the direction of $p_\perp$. Our main assumption states that the

s-quark obtains its required large $k_\perp$ by multiple scattering off quarks and gluons. Due to its nonzero mass it becomes polarized in this process. One can find many different subprocesses contributing to the s-quark scattering, it is even hard to classify the diagrams due to still rather low momentum transfers. We approximate the procedure by assuming the scattering off external gluonic field of the form

$$\Phi^a(\vec{q}) = \frac{4\pi g}{|\vec{q}|^2} I^a, \quad a = 1, \ldots, 8,$$

with g — the quark-gluon coupling constant, $\vec{q}$ — the momentum transfer and I^a — an 8-component vector characterizing the external coloured field. Polarization appears already in the second order of perturbation calculation, in analogy to the electron scattering off external field [53], and reads

$$\mathcal{P} = \frac{2C\alpha_s m_q |\vec{k}|}{\varepsilon^2} \frac{\sin^3 \theta/2 \cdot \ln \sin \theta/2}{\left(1 - \frac{\vec{k}^2}{\varepsilon^2} \sin^2 \theta/2\right) \cos \theta/2} \cdot \hat{\nu}, \tag{6.1}$$

where $C = 1/2(d^{abc}I^aI^bI^c)/(I^aI^a)$, $\alpha_s = \frac{g^2}{4\pi}$, m_q, $\vec{k}$, ε and θ are the mass, the momentum, the energy and the scattering angle of the quark. The unit vector $\hat{\nu} = \frac{\vec{k}_i \times \vec{k}_f}{|\vec{k}_i \times \vec{k}_f|}$ points in the direction perpendicular to the scattering plane. For positive C the expression multiplying $\hat{\nu}$ is negative (see Fig. 26) consequently the quark is polarized in the direction opposite to $\hat{\nu}$.

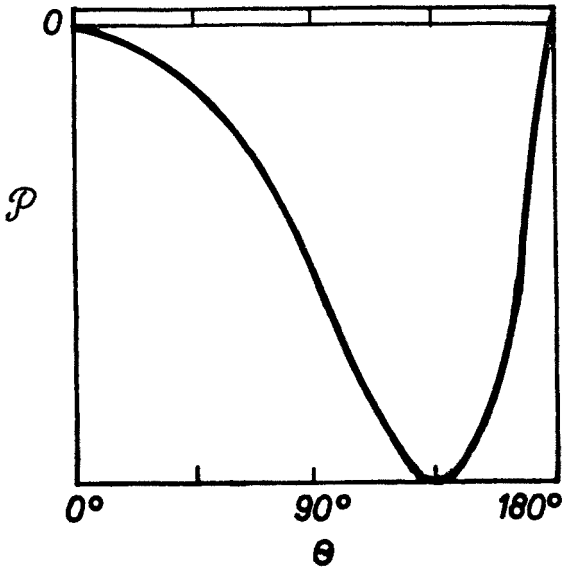

Fig. 26. The quark polarization as a function of the scattering angle in arbitrary units

As we have already mentioned, there is no reason to break the calculation at the second order. Instead of computing higher order diagrams we compared Eq. (6.1) with the exact solution of Dirac equation in external field [54]. Both results give qualitatively the same result, thus we use Eq. (6.1) as a guidance in estimating the effect.

Let us study the structure of Eq. (6.1) in detail. The mass of the strange quark plays a crucial role. For $m = 0$ the polarization vanishes, consequently one does not expect the protons to get polarized, in agreement with experiment [55] (the proton polarization comes out approximately zero also from various quark-diquark recombinations which wash out the quark polarization [56]). On the other hand the mass dependence of Eq. (6.1) implies that the heavy baryons containing c, b, ... quarks should show up even stronger polarization e.g. Λ_c is expected to polarize to negative values with increasing $p_\perp$ and the curves should be even steeper than in the case of Λ. The last statements assume that the c, b, ... sea does not differ much in shape from s-quark sea [57].

The transverse momentum dependence is clearly seen in Fig. 26. Increasing $k_\perp$ means changing θ between 0° and 90°. In this range the absolute value of polarization grows — the major success of the proposed mechanism. The exact value of polarization is not fixed — it depends in particular on α_s and the strength of the external field kept in the constant C.

Eq. (6.1) does not produce strong dependence on Feynman x. The momentum of the Λ is essentially given by that of the diquark. Our statement concerns however directly produced Λ's. The others being the decay products of other resonances (Σ, Y*, ...) populate lower x_Λ and may not be polarized [58]. One should therefore see some increase of polarization of the total Λ sample with increasing x_Λ. This behaviour follows also from kinematics. At $x_\Lambda = 0$ $\mathscr{P}(\Lambda) = 0$ so it must vary with x_Λ if total polarization is nonzero.

Once the mechanism for polarizing the s-quark is fixed, the polarization of other hyperons follows from their spin-flavour wave function. One expects $\mathscr{P}(\Sigma) = -1/3\mathscr{P}(\Lambda)$ (in the Σ^0 wave function the ud-diquark is in $S = I = 1$ state). This relation holds experimentally without the factor 1/3 [58]. This may be a consequence of the fact that the ud valence diquark, being very relativistic and on mass shell, prefers $S_z = 1$ spin projection over $S_z = 0$ [59]. In such a case $\mathscr{P}(\Sigma) \approx -\mathscr{P}(\Lambda)$. The lack of factor 1/3 can be also attributed to the already used argument of resonance production [56]. The are more direct Σ's than Λ's, for instance, the Y*, which has considerable production cross-section, decays in 88% into Λ and only in 12% into Σ. In the Ξ both strange quarks feel the external field, consequently both of them get polarized. One expects $\mathscr{P}(\Xi) \geqslant \mathscr{P}(\Lambda)$ (both are negative), the equality occurring for 100% polarization of the strange quark.

The energy dependence of Eq. (6.1) requires that the s-quark is slow, otherwise the polarization would be negligible. This is the reason why $\bar{\Lambda}$ is not polarized. In the proton induced reactions all its valence quarks come from the proton sea. To build up a finite $x_{\bar{\Lambda}}$ the $\bar{s}$-quark energy has to be large, on the average, and therefore the $\bar{\Lambda}$ polarization vanishes (for $x_{\bar{\Lambda}} = 0$ $\mathscr{P}(\bar{\Lambda}) = 0$ for kinematical reasons).

The idea of multiple quark scattering can be implemented in semiinclusive processes like [60]

$$K^-p \to K\bar{K}\Lambda + \text{pions} \tag{6.2a}$$

$$K^-p \to \Lambda + \text{pions} \tag{6.2b}$$

in which the flow of strangeness is exactly traced. In both reactions (6.2) one looks at the Λ polarization in the proton hemisphere. In the process (6.2a) the incident kaon scatters predominantly by a small angle, therefore the s-quark which builds up the Λ in the proton hemisphere comes from the proton sea. One expects thus polarization increasing (in magnitude) with $p_\perp$ negative with respect to the axis $\hat{\nu} = \vec{k}_i \times \vec{k}_f$, in analogy to the inclusive cases discussed so far. In the process (6.2b) however, the strange quark of the kaon has to turn back in order to build up a Λ in the proton hemisphere. It is then also polarized according to Eq. (6.1) and the absolute value of polarization increases with $p_\perp$ ($p_\perp = 0$ corresponds to the scattering by 180° in Fig. 26). In this case however the normal vector $\vec{\nu}$ changes sign because of $\vec{k}_i$ which points now in the direction of the incident kaon. Thus the polarization shows similar behaviour as in the process (6.2a) but is now positive (see Fig. 27)!

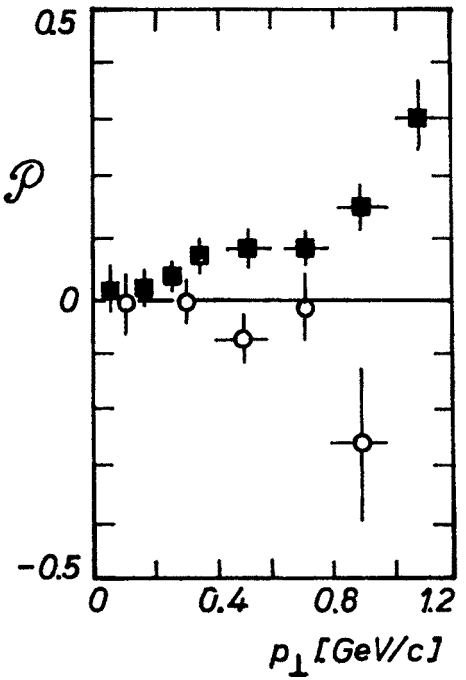

Fig. 27. The Λ polarization in the processes $K^-p \to K\bar{K}\Lambda$ + pions (circles) and $K^-p \to \Lambda$ + pions (squares) as a function of transverse momentum

To our astonishment the proposed mechanism works also in exclusive processes where simple quark diagrams are expected to dominate. Strong Λ (Σ) polarization which goes to large negative (positive) values with increasing $p_\perp$ has been measured [61] in the process $pp \to \Lambda\bar{\Lambda}$ ($pp \to \Sigma\bar{\Sigma}$). The phenomenon with opposite polarizations noticed for the reactions (6.2) shows up in the exclusive channels [62]

$$\pi^+p \to K^+\Sigma^+$$

$$K^-p \to \pi^-\Sigma^+.$$

In the first reaction Σ^+ is positively polarized, as in the inclusive production, whereas in the second one the Σ^+ polarization is negative.

To summarize this subsection we have shown a simple mechanism of baryon polarization based on the multiple quark scattering idea. It is worth noting that the proposed approach can be easily incorporated in the known models of low and intermediate $p_\perp$ scattering.

B. Other models

We review briefly two models [56, 63] which describe the phenomenon of hyperon polarization.

In the semiclassical picture of Anderson, Gustafson and Ingelman [56] the ud diquark in the $S = I = 0$ and colour 3 state, which survives the collision as a unit, stretches a colour flux tube. The $s\bar{s}$ pair, needed to build a Λ, is produced in the gluonic field with local transverse momentum, energy, and angular momentum conservation. This means that the s and $\bar{s}$ quark have opposite transverse momenta $\vec{k}_\perp$ and $-\vec{k}_\perp$ and

$$\kappa l = 2\sqrt{m^2+k_\perp^2},$$

where κ is the energy density in the colour tube and l — the distance between the produced strange quarks (see Fig. 28). The resulting orbital angular momentum

$$|\vec{L}| = l \cdot |\vec{k}_\perp| = 2|\vec{k}_\perp| \cdot \frac{\sqrt{m_s^2+k_\perp^2}}{\kappa} \tag{6.3}$$

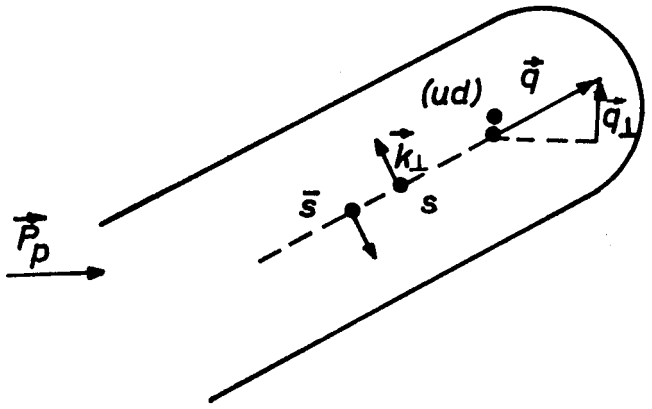

Fig. 28. The colour flux tube in the model of Ref. [56]

is assumed to be compensated by the spin of the produced $s\bar{s}$ pair. Because $\vec{k}_\perp$ points in most cases in the direction of the transverse momentum $\vec{p}_\perp$ of the Λ, $\vec{L}$ is parallel to the direction $\vec{q}_\perp \times \vec{k}_\perp$ (as in Fig. 28) and consequently the spin of the s-quark is antiparallel to this direction. This qualitative argument can be cast in a definite form which expresses the spin-orbital angular momentum or, due to Eq. (6.3), spin-tranverse momentum correlation. Assuming additionally some form of the transverse momentum distribution of the

ud-diquark and the s-quark one can compute the behaviour of Λ polarization as a function of $p_\perp$ (see Fig. 29). Its exact shape depends on a few parameters but it is seen that one is able to reproduce the trend of the data.

The polarization of other hyperons follows again from the spin-flavour part of their wave functions. The model may need additional assumptions in the case of Ξ where two strange quarks are produced. One also does not explain why the Λ is sometimes polarized in the opposite direction as it is the case in the process (6.2b).

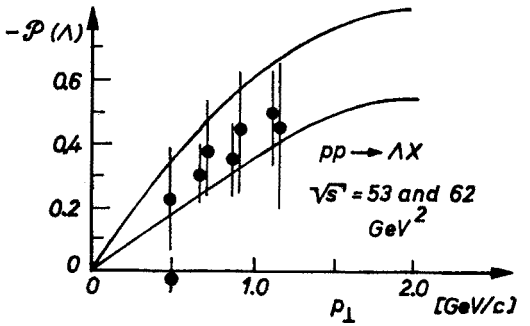

Fig. 29. The Λ polarization in the model of Ref. [56]. The allowed region lies between the two curves

Another model, which also uses a quasi-classical effect to describe the polarization phenomena was proposed by DeGrand and Miettinen [63]. The spin ordering occurs here after the collision in the recombination process. Let us present the argument on the Λ hyperon where only the spin of the strange quark matters. In order to recombine fast valence diquark with the slow strange sea quark one needs forces which accelerate the last one to momenta typical for a valence quark ($x_{s/\Lambda} \approx 1/3$, see Fig. 30). The quark spin s feels then the effect of Thomas precession [64] which manifests itself through a term in the effective Hamiltonian

$$U = \vec{s} \cdot \vec{\omega}_T, \tag{6.4}$$

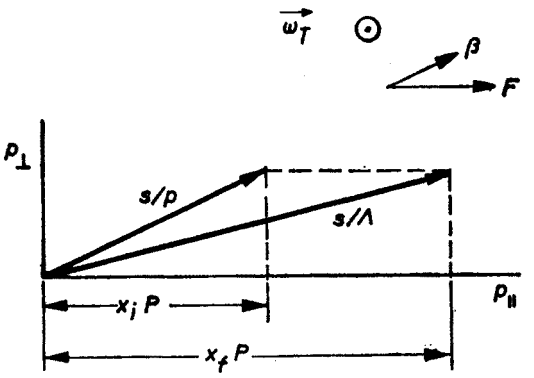

Fig. 30. The momentum diagram in the recombination model of Ref. [63]

where the Thomas precession frequency

$$\vec{\omega}_T \sim \frac{1}{m_s} \vec{F} \times \vec{v}.$$

$\vec{F}$ is the operating colour force and $\vec{v}$ — the quark velocity. The direction of $\vec{\omega}_T$ is easy to find (see Fig. 30) and it is argued that the spin s points in direction opposite to $\vec{\omega}_T$ in order to minimize the interaction term (6.4). An approximate estimate of the effect suggests a correct $p_\perp$ and x dependence. The Thomas precession acts not only on the strange quark but on the diquark as well. This has crucial influence on the polarization of other hyperons, in which the diquark is not in $S = 0$ state. In the case of Σ it results in the enhancement of the diquark state with $S_z = 1$ over $S_z = 0$. As a consequence one is able to obtain the experimentally supported relation $\mathscr{P}(\Sigma) = -\mathscr{P}(\Lambda)$ (without the previous factor 1/3). Assuming two independent contributions to the polarization (although both originating from the Thomas precession) one from the slowed down or speeded up quarks, the other one from the diquarks the authors construct a table of polarizations in all possible, inclusive transitions. As a matter of fact this table is independent of the proposed dynamical mechanism of polarization and can be regarded as a two variable parametrization of all polarizations following from the recombination model with SU(6) symmetric baryon wave functions.

One notices several differences in the predictions when comparing this model with the one proposed in the previous subsection. Among the most decisive ones is the statement on Λ_c polarization. It is supposed to be polarized oppositely to Λ in the last model. The authors also expect strong Λ polarization in $K^- \to \Lambda$ in the K^- hemisphere. This is not the case in our model where the strange quark is on the average too fast to get polarized. The Thomas precession model does not account for the change of polarization sign in the reactions (6.2).

7. *Summary and conclusions*

We attempted to present the importance of spin effects in large $p_\perp$ hadronic collisions. Two types of processes were investigated in detail.

In elastic scattering at large angles one is dealing with three potentially important contributions, each coming from a different region of phase space. They are weighted by the hadronic wave functions $\Psi(x, k_\perp)$. The short distance amplitudes emerge from x and far from its limiting values ($x \neq 0, 1$) and large $k_\perp$. They are constructed in analogy to the dominant meson formfactor amplitudes. The end-point contribution requires x close to the limits and small intrinsic transverse momenta. Finally the Landshoff pinch diagrams get the support from small $k_\perp$ and x's constrained by the condition stating that the momentum fractions x of all constituents are equal to each other to $O\left(\frac{1}{Q}\right)$. All contributions form a small part of the total cross-section, in the first two cases they are suppressed by the wave

function $\Psi(x, k_\perp)$ which vanishes for $k_\perp \to \infty$ or $x \to 1$, in the last case the condition put on x cuts out a small region of phase space.

In the situation where the relative normalization of these contributions is unknown we investigate phenomenological consequences of each term. The behaviour of the differential cross-section shows that the pinch diagrams dominate the $|t| \ll s$ region. The dimensional counting rules which follow from both short distance and end-point diagrams work well at angles close to 90°. In this region the predictions concerning the spin-spin asymmetries differ significantly when calculated in each of the mentioned approximations. At present momentum transfers only the end-point calculation accounts for the large value of A_{nn}.

The above analysis proves that the spin observables carry nontrivial information, sometimes more clear than that contained in the cross-sections. In the considered case the reason for this has a simple physical interpretation. In the large angle scattering process the helicities of the final hadrons are combined from finite contributions of all quarks (this is to be contrasted with e.g. momentum transfer dependence of the amplitude, where softly interacting constituents contribute only infinitesimally). It matters therefore, when calculating spin observables, what is the structure of each subinteraction in the diagram. In particular one is able to distinguish how many quark lines take part in the hard collision. The dominance of the end-point contribution in elastic scattering implies that only part of the diagram (one quark line in each hadron) exchanges large momentum.

As a "byproduct", when comparing different types of elastic diagrams, we obtained the extension of the Drell-Yan-West relations to this process. Definite form of the elastic amplitude which also emerges in this approximation agrees very well with all large angle elastic data. It can be also easily applied to other exclusive channels.

Another type of process where spin is known to play an important role is hyperon polarization in large transverse momentum inclusive production. Here the theoretical situation is less clear. It turns out a posteriori that the measured phenomena are in fact "intermediate $p_\perp$" effects where soft interactions play dominant role. Therefore we limit ourselves to a qualitative description. A simple mechanism based on multiple scattering of quarks is proposed. It accounts for the polarization of nonzero mass quarks and consequently explains many polarization phenomena in inclusive production. It works also when applied to exclusive channels.

The two described examples of spin effects in hadron-hadron collisions [65] are intended to show how important they are at large momentum transfers. Because of dominance of relatively simple diagrams in this region one gets direct information on the underlying chromodynamic interaction. Finally we think that the two surprising results of the spin physics in the last few years found their explanation.

The author would like to thank A. Białas for continuous interest in this work and many valuable remarks.

Helpful discussions with S. Brodsky, G. Cocho, A. Kotański, H. Lipkin, M. Moreno, W. Ochs and L. Stodolsky are also acknowledged.

APPENDIX A

pp amplitudes and spin observables

Out of 16 helicity amplitudes in NN → NN only 5 are independent. Using the Jacob-Wick convention [66] and assuming the scattering in the xz plane ($\varphi = 0$) parity conservation means

$$\mathcal{M}_{\gamma\delta\alpha\beta}(s, t) = (-)^{\alpha-\beta-\gamma+\delta}\mathcal{M}_{-\gamma-\delta-\alpha-\beta}(s, t).$$

Time reversal invariance reduces further the number of independent amplitudes to six

$$\mathcal{M}_{\gamma\delta\alpha\beta}(s, t) = (-)^{\alpha-\beta-\gamma+\delta}\mathcal{M}_{\alpha\beta\gamma\delta}(s, t).$$

Identical particle relation reads

$$\mathcal{M}_{+++-}(s, t) = -\mathcal{M}_{++-+}(s, t).$$

The 5 independent amplitudes in pp → pp are chosen to be

$$\begin{aligned}
\Phi_1(s, t) &= \mathcal{M}_{++++}(s, t)+\mathcal{M}_{++++}(s, u)\\
\Phi_2(s, t) &= \mathcal{M}_{++--}(s, t)+\mathcal{M}_{++--}(s, u)\\
\Phi_3(s, t) &= \mathcal{M}_{+-+-}(s, t)-\mathcal{M}_{-++-}(s, u)\\
\Phi_4(s, t) &= \mathcal{M}_{-++-}(s, t)-\mathcal{M}_{+-+-}(s, u)\\
\Phi_5(s, t) &= \mathcal{M}_{+++-}(s, t)-\mathcal{M}_{+++-}(s, u).
\end{aligned} \tag{A.1}$$

The spin-spin asymmetries are defined

$$A_{ii} = \frac{d\sigma/dt(\uparrow\uparrow)+d\sigma/dt(\downarrow\downarrow)-d\sigma/dt(\uparrow\downarrow)-d\sigma/dt(\downarrow\uparrow)}{d\sigma/dt(\uparrow\uparrow)+d\sigma/dt(\downarrow\downarrow)+d\sigma/dt(\uparrow\downarrow)+d\sigma/dt(\downarrow\uparrow)},$$

where i = n means the initial spin projected normal to the scattering plane (y-axis), $i = 1$ — in the direction of motion (x-axis) and i = s — sideways (z-axis). In terms of the helicity amplitudes Φ_j ($j = 1, \ldots, 5$) they read

$$\begin{aligned}
A_{nn} &= 2 \cdot \mathrm{Re}\,(\Phi_1 \cdot \Phi_2^* - \Phi_3 \cdot \Phi_4^* + 2|\Phi_5|^2)/D,\\
A_{ss} &= 2 \cdot \mathrm{Re}\,(\Phi_1 \cdot \Phi_2^* + \Phi_3 \cdot \Phi_4^*)/D,\\
A_{ll} &= (-|\Phi_1|^2 - |\Phi_2|^2 + |\Phi_3|^2 + |\Phi_4|^2)/D,\\
A_{sl} &= 2\,\mathrm{Re}\,[(\Phi_1 + \Phi_2 - \Phi_3 + \Phi_4) \cdot \Phi_5^*]/D,
\end{aligned} \tag{A.2}$$

where

$$D = |\Phi_1|^2 + |\Phi_2|^2 + |\Phi_3|^2 + |\Phi_4|^2 + 4|\Phi_5|^2.$$

The polarization $\mathscr{P}$ is given by

$$\mathscr{P} = -2\,\mathrm{Im}\,[(\Phi_1+\Phi_2+\Phi_3-\Phi_4)\Phi_5^*]/D.$$

At $\theta_{\mathrm{c.m.}} = 90°$ one may use $\Phi_3 = -\Phi_4$ to show that

$$A_{nn}-A_{ll}-A_{ss} = 1.$$

APPENDIX B

The neutron-proton elastic amplitudes

There are 5 independent helicity amplitudes $\mathscr{M}_{\gamma\delta\alpha\beta}$ in analogy to pp elastic scattering. Assuming the quark interchange they read

$$\Phi_1(s,t) = \tfrac{1}{18}\,[14M_{++++}(s,t)+22M_{+--+}(s,t)+17M_{++++}(s,u)-8M_{+--+}(s,u)]$$

$$\Phi_2(s,t) = \tfrac{1}{18}\,[-8M_{++--}(s,t)+25M_{++--}(s,u)]$$

$$\Phi_3(s,t) = \tfrac{1}{18}\,[22M_{++++}(s,t)+14M_{+--+}(s,t)-25M_{-++-}(s,u)]$$

$$\Phi_4(s,t) = \tfrac{1}{18}\,[-8M_{-++-}(s,t)-17M_{+--+}(s,u)+8M_{++++}(s,u)]$$

$$\Phi_5(s,t) = \tfrac{1}{18}\,[-8M_{+++-}(s,t)-25M_{+++-}(s,u)].$$

In the case of s-channel helicity conservation in the whole process [15, 16] only $M_{++++} = -M_{-++-} = f$ survive giving

$$\Phi_1(s,t) = \tfrac{1}{18}\,[14f(s,t)+17f(s,u)]$$

$$\Phi_3(s,t) = \tfrac{1}{18}\,[22f(s,t)+25f(s,u)]$$

$$\Phi_4(s,t) = \tfrac{1}{18}\,[8f(s,t)+8f(s,t)]$$

$$\Phi_5(s,t) = \Phi_2(s,t) = 0.$$

The leading order helicity amplitudes in the end-point region are obtained as described in Section 4. The result is

$$\Phi_1(s,t) = \tfrac{1}{18}\,\{[-8+f(s,t)]M_{++++}(s,t)+4f'(s,t)M_{-++-}(s,t)$$
$$+[25+f'(s,u)]M_{++++}(s,u)+f'(s,u)M_{-++-}(s,u)\}G_{\mathrm{M}}(t)G_{\mathrm{M}}(u)$$

$$\Phi_2(s,t) = \tfrac{1}{18}\,\{-4f'(s,t)M_{++++}(s,t)+[14+h(s,t)]M_{-++-}(s,t)$$
$$-f'(s,u)M_{++++}(s,u)+[8-h'(s,u)]M_{-++-}(s,u)\}G_{\mathrm{M}}(t)G_{\mathrm{M}}(u)$$

$$\Phi_3(s,t) = \tfrac{1}{18}\,\{f(s,t)M_{++++}(s,t)+4f'(s,t)M_{-++-}(s,t)$$
$$-f'(s,u)M_{++++}(s,u)-[17+h'(s,u)]\cdot M_{-++-}(s,u)\}G_{\mathrm{M}}(t)G_{\mathrm{M}}(u)$$

$$\Phi_4(s,t) = \tfrac{1}{18}\{4f'(s,t)M_{++++}(s,t)+[14+h(s,t)]M_{-++-}(s,t)$$
$$-f'(s,u)M_{++++}(s,u)-f'(s,u)M_{-++-}(s,u)\}G_M(t)G_M(u)$$

$$\Phi_5(s,t) = \tfrac{1}{18}\{k(s,t)M_{++++}(s,t)+l(s,t)M_{-++-}(s,t)$$
$$-k'(s,u)\cdot M_{++++}(s,u)-l'(s,u)M_{-++-}(s,u)\}G_M(t)G_M(u)$$

$$f(s,t) = 2\sin^2\theta_{GJ}(7+4\sin^2\theta_{GJ}), \quad k = -\sin\theta_{GJ}\cos\theta_{GJ}(15+8\cos^2\theta_{GJ})$$

$$f' = -2\cos^2\theta_{GJ}\sin^2\theta_{GJ}, \quad k' = -\sin\theta_{GJ}\cos\theta_{GJ}(3+2\cos^2\theta_{GJ})$$

$$h = -2\sin^2\theta_{GJ}(15-4\sin^2\theta_{GJ}), \quad l = -\sin\theta_{GJ}\cos\theta_{GJ}(7+8\cos^2\theta_{GJ})$$

$$h' = 2\sin^2\theta_{GJ}(7+\sin^2\theta_{GJ}), \quad l' = \sin\theta_{GJ}\cos\theta_{GJ}(5+2\cos^2\theta_{GJ})$$

$$M_{++++}(s,t) = 4\pi\alpha_s\frac{s}{u}$$

$$M_{-++-}(s,t) = 4\pi\alpha_s\frac{t}{u}.$$

The spin observables are defined and expressed in terms of helicity amplitudes as in the pp elastic scattering (Appendix A).

REFERENCES

[1] G. P. Lepage, S. J. Brodsky, *Phys. Lett.* **87B**, 359 (1979); *Phys. Rev. Lett.* **43**, 545 (1979); Erratum *ibid.* **43**, 1625 (1979); *Phys. Rev.* **D22**, 2157 (1980); *Phys. Scr.* **23**, 945 (1981); A. V. Efremov, A. V. Radyushkin, *Teor. Mat. Fiz.* **42**, 147 (1980); Dubna preprints E2-12384 (1979), E2-80-521 (1980); A. Duncan, A. H. Mueller, *Phys. Rev.* **D21**, 1636 (1980); *Phys. Lett.* **90B**, 159 (1980).

[2] P. V. Landshoff, *Phys. Rev.* **D10**, 1024 (1974); Preprint DAMTP 78/19 (1978); P. Cvitanovic, *Phys. Rev.* **D10**, 338 (1974).

[3] S. D. Drell, M. Yan, *Phys. Rev. Lett.* **24**, 181 (1970); G. West, *Phys. Rev. Lett.* **24**, 1206 (1970).

[4] J. Szwed, Jagellonian University preprint TPJU-18/81 (1981).

[5] See Refs. [15, 16, 31, 52, 56, 63] and C. Avilez, G. Cocho, M. Moreno, *Phys. Rev.* **D24**, 634 (1981); J. de Sa Borges, E. Candotti, G. Cocho, J. A. Mignaco, Rio de Janeiro preprint (1981); G. Preparata, J. Soffer, *Phys. Lett.* **86B**, 304 (1979); G. F. Wolters, *Phys. Rev. Lett.* **45**, 776 (1980); M. G. Doncel, Barcelona preprint UAB-FT-65 (1980); M. Matsuda, H. Suemitsu, W. Watari, M. Yonezawa, Hiroshima preprint HUPD-8110 (1981); M. Anselmino, Westfield Coll. preprint (1981); See also Talks by M. G. Doncel, M. Moreno, G. Preparata, and G. F. Wolters at the Conf. HEPPBPT, Lausanne 1980.

[6] J. R. O'Fallon et al., *Phys. Rev. Lett.* **39**, 733 (1977); D. G. Crabb et al., *Phys. Rev. Lett.* **41**, 1257 (1978); D. A. Crosbie et al., Ann Arbor preprint UMHE 80-2 (1980).

[7] G. Bunce et al., *Phys. Rev. Lett.* **36**, 1113 (1978); S. Erhan et al., *Phys. Lett.* **82B**, 301 (1979); M. L. Facinni-Turluer et al., *Z. Phys.* **C1**, 19 (1979); F. Lomano et al., *Phys. Rev. Lett.* **43**, 1905 (1979); K. Rayadhuri et al., *Phys. Lett.* **90B**, 313 (1980); K. Heller et al., *Phys. Lett.* **68B**, 480 (1977); K. Heller et al., *Phys. Rev. Lett.* **41**, 607 (1978); See also review talk: G. Bunce, in Proc. of the Conf. HEPPBPT, Lausanne 1981.

[8] G. P. Lepage, S. J. Brodsky, *Phys. Lett.* **87B**, 359 (1979); *Phys. Lett.* **91B**, 239 (1980); A. V. Efremov,

A. V. Radyushkin, *Teor. Mat. Fiz.* **42**, 147 (1980); Dubna preprint E2 12384 (1979); *Phys. Lett.* **94B**, 245 (1980).
[9] G. Altarelli, G. Parisi, *Nucl. Phys.* **B126**, 298 (1977).
[10] G. Farrar, D. Jackson, *Phys. Rev. Lett.* **43**, 246 (1979) and Ref. [8].
[11] G. P. Lepage, S. J. Brodsky, second paper in Ref. [1].
[12] M. D. Mestayer, SLAC-Report No **214** (1978) and references therein.
[13] S. J. Brodsky, G. Farrar, *Phys. Rev. Lett.* **31**, 1153 (1973); A. V. Matveev, R. M. Muradyan, A. V. Tavkhelidze, *Lett. Nuovo Cimento* **7**, 19 (1973).
[14] G. P. Lepage, S. J. Brodsky, *Phys. Rev.* **D22**, 2157 (1980).
[15] G. R. Farrar, S. Gottlieb, D. Sivers, G. Thomas, *Phys. Rev.* **D20**, 202 (1979).
[16] S. J. Brodsky, C. E. Carlson, H. Lipkin, *Phys. Rev.* **D20**, 2278 (1979); See also: S. J. Brodsky, G. P. Lepage, in Proc. of the Conf. HEPPBPT, Lausanne 1981.
[17] J. Szwed, Jagellonian University preprint TPJU-13/80 (1980).
[18] A. Donnachie, P. V. Landshoff, *Z. Phys.* **C2**, 55 (1979).
[19] J. L. Martman et al., *Phys. Rev. Lett.* **39**, 975 (1977); S. Conetti et al., *Phys. Rev. Lett.* **41**, 924 (1978); M. Dekerret et al., *Phys. Lett.* **68B**, 374 (1977); W. Faissler et al., Cornell preprint CLNS 80/471 (1980).
[20] G. Farrar, C. C. Wu, *Nucl. Phys.* **85**, 50 (1975).
[21] R. P. Feynman, *Photon-Hadron Interaction*, Benjamin 1972.
[22] X. Artru, *Phys. Rev.* **D24**, 1662 (1981); Orsay preprint LPTHE 82/01 (1982).
[23] J. F. Gunion, S. J. Brodsky, R. Blankenbecler, *Phys. Rev.* **D8**, 287 (1973); D. Sivers, R. Blankenbecler, S. J. Brodsky, *Phys. Rep.* **23C**, 1 (1976).
[24] T. T. Chou, C. N. Yang, *Phys. Rev.* **170**, 1591 (1968); D. Horn, M. Moshe, *Nucl. Phys.* **B48**, 557 (1972).
[25] J. Szwed, *Phys. Rev.* **D25**, 735 (1982).
[26] M. V. Allaby et al., *Phys. Lett.* **25B**, 156 (1967); G. Cocconi et al., *Phys. Rev.* **138**, 1653 (1965).
[27] J. D. Bjorken, private communication.
[28] J. L. Stone et al., *Nucl. Phys.* **B143**, 1 (1979).
[29] L. Backman et al., contribution to the EPS Conference, Lisbon 1981.
[30] R. Almas et al., *Phys. Lett.* **93B**, 199 (1980).
[31] J. Szwed, *Phys. Lett.* **93B**, 485 (1980).
[32] K. Gottfried, J. D. Jackson, *Nuovo Cimento* **33**, 309 (1964).
[33] T. L. Trueman, G. C. Wick, *Ann. Phys.* **26**, 322 (1964); G. Cohen-Tannoudji, A. Morel, M. Navelet, *Ann. Phys.* **46**, 239 (1968).
[34] A. Białas, A. Kotański, K. Zalewski, *Nucl. Phys.* **B28**, 1 (1971).
[35] A. Kotański, *Acta Phys. Pol.* **29**, 699 (1966); **30**, 629 (1966).
[36] I. P. Auer et al., paper contributed to XX Int. Conf. on HEP, Madison 1980.
[37] See e.g. J. J. J. Kokkedee, *The Quark Model*, Benjamin 1969.
[38] A. Bodek et al., *Phys. Rev. Lett.* **30**, 1087 (1973); J. S. Poucher et al., *Phys. Rev. Lett.* **32**, 118 (1974).
[39] P. Allen et al., *Phys. Lett.* **103B**, 71 (1981).
[40] G. Baum et al., contribution to the XX Int. Conf. on HEP, Wisconsin 1980.
[41] I. A. Schmidt, R. Blankenbecler, *Phys. Rev.* **D16**, 1318 (1977); F. E. Close, R. G. Roberts, Rutherford preprint RL-80-058 (1980).
[42] R. Carlitz, *Phys. Lett.* **58B**, 345 (1975); J. Kaur, *Nucl. Phys.* **B128**, 219 (1977).
[43] See Ref. [21]; J. D. Bjorken, E. A. Paschos, *Phys. Rev.* **185**, 1975 (1965); **D1**, 3151 (1970).
[44] G. R. Farrar, D. R. Jackson, *Phys. Rev. Lett.* **35**, 1416 (1975); A. I. Vainshtein, V. I. Zakharov, *Phys. Lett.* **72B**, 368 (1978); E. L. Berger, S. J. Brodsky, *Phys. Rev. Lett.* **42**, 940 (1979); G. Parisi, *Phys. Lett.* **84B**, 225 (1979).
[45] J. Szwed, Jagellonian University preprint TPJU-19/81 (1981).
[46] Ref. [1]; A. H. Mueller, *Phys. Rep.* **73C**, 239 (1981); A. Duncan, *Phys. Scr.* **23**, 961 (1981).
[47] P. V. Lanshoff, D. J. Pritchard, *Z. Phys.* **C6**, 69 (1980).

[48] K. Wilson, Cornell Report No LNS-64-15 (1964); *Phys. Rev.* **179**, 1499 (1969).
[49] V. Sudakov, *Zh. Eksp. Teor. Fiz.* **30**, 87 (1956) [*JETP* **3**, 65 (1956)].
[50] A. H. Mueller, *Phys. Rep.* **73C**, 239 (1981).
[51] R. D. Field, R. Gupta, S. Otto, L. Chang, Gainesville preprint UFTP-80-21; F. M. Dittes, A. V. Radyushkin, Dubna preprint E2-80-688.
[52] J. Szwed, *Phys. Lett.* **105B**, 403 (1981); Talk in the Proc. of the IV Warsaw Symposium, Kazimierz 1981.
[53] A. W. McKinley, H. Feshbach, *Phys. Rev.* **74**, 1759 (1948); R. H. Dalitz, *Proc. Roy. Soc.* (London) **A206**, 509 (1951).
[54] N. F. Mott, H. S. N. Masey, *Theory of Atomic Collisions*, (III ed.) Oxford.
[55] R. Polvado, Talk at HEPPBPT Conference (1978).
[56] B. Anderson, G. Gustafson, G. Ingelman, *Phys. Lett.* **85B**, 417 (1979).
[57] For other point of view see: S. J. Brodsky, P. Hoyer, C. Peterson, N. Sakai, *Phys. Lett.* **93B**, 451 (1980).
[58] O. E. Overseath, in Proc. of the Conf. HEPPBPT, Lausanne 1980.
[59] G. Cocho, private communication.
[60] Amsterdam-CERN-Nijmegen-Oxford Coll., Report CERN/EP/Phys. 76-25, submitted to Int. Conf. on HEP, Tbilisi 1976.
[61] H. W. Atherton et al., *Nucl. Phys.* **B69**, 1 (1974).
[62] S. M. Prus et al., *Phys. Rev. Lett.* **23**, 188 (1969); K. S. Han et al., *Phys. Rev. Lett.* **24**, 1353 (1970); E. N. May et al., Argonne preprint ANL-HEP-CP-80-37 (1980).
[63] T. De Grand, H. I. Miettinen, *Phys. Rev.* **D23**, 1227 (1981); Helsinki preprint HU-TFT-81-35 (1981).
[64] L. T. Thomas, *Philos. Mag.* **3**, 1 (1927); also in J. D. Jackson, *Classical Electrodynamics*, II ed., J. Wiley and Sons, 1978.
[65] For review papers on these and other spin phenomena see: C. Bourrely, E. Leader, J. Soffer, *Phys. Rep.* **59C**, 98 (1980); A. D. Krisch, Lecture at 1981 Orbis Scientiae at Coral Gables; A. Yokosawa, *Phys. Rep.* **64C**, 50 (1980).
[66] M. Jacob, G. C. Wick, *Ann. Phys.* **7**, 404 (1959).